

Map-Assisted Power Allocation and Constellation Design for mmWave WDM with OAM in Short-Range LOS Environment

Yuan Wang, Chen Gong, and Zhengyuan Xu

Abstract

Consider a system that integrates positioning and single-user millimeter wave (mmWave) communication, where the communication part adopts wavelength division multiplexing (WDM) and orbital angular momentum (OAM). This paper addresses the power allocation and high dimensional constellation design in short-range line-of-sight (LOS) environment, with stable communication links. We propose a map-assisted method to replace online estimation, feedback and computation with the look-up table searching. We explore the possibility of using a few patterns in the maps, and investigate the performance loss of using the optimal solution of one position for other positions. For power allocation, we first characterize the performance loss outside the OAM beam regions with only plane waves, and figure out that the loss is always small. However, in OAM beam regions, the performance loss has similar characteristics only at some specific positions. Based on numerical results, we illustrate that a few patterns can be adopted for all receiver locations in the map. We also investigate high dimensional constellation design, and prove that a fixed constellation can be adopted for the positions where the channel matrices are sufficiently close to be proportional. Similarly, we figure out that the constellation design for all receiver locations can be represented by a few constellation sets.

Index Terms

Millimeter wave communication, power allocation, high dimensional constellation, wavelength division multiplexing, short-range line-of-sight.

This work was supported by Key Program of National Natural Science Foundation of China (Grant No. 61631018), Key Research Program of Frontier Sciences of CAS (Grant No. QYZDY-SSW-JSC003), and the Fundamental Research Funds for the Central Universities.

Yuan Wang, Chen Gong, and Zhengyuan Xu are with Key Laboratory of Wireless-Optical Communications, Chinese Academy of Sciences, University of Science and Technology of China, Hefei, Anhui 230027, China. Email: wangy001@mail.ustc.edu.cn; {cgong821,xuzy}@ustc.edu.cn.

I. INTRODUCTIONS

Currently, intelligent terminals are becoming more and more widely deployed, which provide not only positioning, tracking and other sensing services, but also high-speed communication services [1], [2]. However, with the development of communication technologies, the demand for spectrum resource is increasing. Such trend calls for high-frequency spectrum like millimeter wave (mmWave) and Tera Hertz (THz) [3], [4]. In this work, we mainly consider mmWave spectrum. Compared with sub-6GHz communication, mmWave communication can occupy wider spectrum resource (30-300 GHz) to guarantee high-speed transmission [5]. On the other hand, orbital angular momentum (OAM), as a new degree of freedom, is applied to mmWave systems to further increase the transmission rate [6]–[10].

Due to the characteristics of beam diffusion and coaxial transmission, OAM is only suitable for short-range line-of-sight (LOS) communication [8], [11]–[13]. Moreover, higher spectrum will lead to larger propagation, penetration and reflection losses [14]–[16], which further limits the application to short-range LOS environment. In most existing mmWave systems, data processing is performed only in a single narrow spectrum [17], [18], and the advantage of mmWave spectrum is not fully utilized [19], [20]. Beneficial from the large link losses, mmWave systems can aggregate the licensed or unlicensed broad spectrum with small external interference to increase transmission rate. In general, broad spectrum communication is combined with wavelength division multiplexing (WDM) technology, which adopts multiple carrier wavelengths to transmit data streams [21]–[24].

For mmWave spectrum communication in sparsely scattered environment, such as conference room and workshop, the influence of multi-path is limited and the LOS path is dominant [25]. Meanwhile, the mmWave propagation shows an apparent quasi-optical property according to experimental measurement [26], [27]. Hence, the mmWave short-range LOS link can be considered as a LOS channel, also called determined channels [15]. Based on the above feature, the link conditions of mmWave communication in short-range LOS environment are only related to the positions of transmitter and receiver [28]. Generally, high accuracy positioning is necessary for some short-range intelligent systems, such as industrial internet and indoor robot. If OAM is adopted, this position information can be used to align the receiving antenna axis with transmitting antenna axis. Certainly, the systems can directly utilize OAM signals to locate and communicate [28], [29].

Motivated by the quasi-static feature and positioning-communication integration, we attempt to configure the communication system based on the transceiver's position. Due to the stable gains for short-range LOS links, the optimal system parameters are determined when the position information is obtained. Hence, we construct a look-up table, which is named as map method, to store the system parameters of all interested positions [30]. Adopting map-assisted approach has two potential advantages: (1) For the system whose positioning service is active, the transmitter and receiver always have position

information. If a communication request appears, the system can directly configure the transmitter and receiver by adopting the parameters stored in the map. Since that there is no need for the time and transmission symbol overhead of channel estimation, channel feedback and real-time optimization, the delay of initial communication establishment will be reduced. (2) The system can solve computationally intensive optimization problems in an offline manner and store the optimization results into the map, which significantly relaxes the real-time computational pressure.

Obviously, the positional quantization will mainly affect the system performance [31]. High quantization accuracy can improve the system performance, but will increase the storage and search complexity. Therefore, it is necessary to simplify the map on a certain performance loss tolerance. And it can be expected that after quantization with certain distortion threshold, there are only a few patterns stored in the map.

This work considers the mmWave WDM with different OAM modes under short-range LOS scenario. We mainly focus on two problems: power allocation from channel capacity perspective, and high dimensional constellation design primarily for improving the detection performance. Considering map-assisted communication systems, we concern that the performance loss caused by position clustering in the map. More specifically, we analyze the metric loss of each problem when the system lies at a certain position but adopts the configuration parameters of another position. For power allocation, we investigate the feasibility of using one power allocation scheme for different receiver locations. Within regions only having plane wave ($l = 0$), we characterize the sum-rate difference under uniform link gain ratio, and figure out that the mmWave WDM system can employ fixed power allocation due to high signal to noise ratio (SNR) in short-range LOS scenario. Combining theoretical analyses with numerical results, we also figure out that there are a few power allocation schemes for the regions multiplexing several OAM modes, which enables the representation of power allocation using a few patterns in a map. Then, we consider the high dimensional constellation design using minimum Euclidean distance (MED) as the performance criterion. To characterize the possibility of assigning few constellation sets to the entire interested positions, we prove that for any position 2, the normalized MED difference of using the constellation of position 1 can be sufficiently small if the channel matrices of positions 1 and 2 are sufficiently close to be proportional. Thus, a fixed constellation can be adopted for plane wave ($l = 0$) only regions due to the uniform link gain ratio. The claim of only a few constellation patterns is supported by the numerical results.

The remainder of this paper is organized as follows. In Section II, we provide the system model, elaborate the features of OAM beams and display the configuration process of map-assisted systems. In Section III, we characterize the power allocation patterns of the region only having plane wave and the region multiplexing several OAM modes, and demonstrate that there may be only a few power

allocation patterns especially under high SNR scenario. In Section IV, we investigate the high dimensional constellation design, and figure out that the same link gain ratio leads to the same constellation, and that the constellation design can be represented by only a few constellation sets in the map. Finally, Section V concludes this paper.

II. SYSTEM MODEL

Consider a short-range LOS mmWave WDM system, which also equips a positioning module, shown in Figure 1. The transmitter and receiver both consist of I different carrier frequencies and assume $I = 3$ in this example. Assume perfect band-pass filter on each carrier to remove the inter-carrier interference. Since the antenna of each carrier frequency can multiplex several OAM modes, the whole system can be regarded as consisting of I parallel mmWave sub-systems. At the transmitter side, we utilize travelling-wave antennas, which is simpler than spiral phase plates (SPP) [7], [8], to generate Laguerre-Gaussian (LG) beams with different OAM modes under coaxial condition [6], [10], [32]. The I sub-systems form an uniform linear array with equal distance d_a . At the receiver side, we adopt uniform circular array (UCA) [33], [34] for detection, where the interval of the centers of any two adjacent antennas is also d_a . Beneficial from the position information, the transmitting and receiving antennas are generally considered to be aligned [8], [13], which can also be realized by tracking schemes [35], [36]. However, the receiver may lie outside the LG beam, which is shown in Figure 1. In these regions, we assume that each sub-system aligns the beam axis with one of the receiving antennas in UCA. Since the whole system loses coaxial condition, we assume that only plane waves ($l = 0$) are transmitted.

We adopt LG method to characterize OAM beams [6], [37]. In cylindrical coordinate, the channel response on the i -th carrier with OAM mode l at any position (r, ϕ, z) can be given by [6], [37]

$$h_i^l(r, \phi, z) = \frac{\sqrt{\zeta_i^l \lambda_i}}{4\pi d_{i,m}^l(z)} \left(\frac{r}{r_{i,max}^l(z)} \right)^{|l|} e^{\frac{(r_{i,max}^l(z))^2 - r^2}{\omega_i^2(z)}} e^{-j \frac{\pi(r^2 - (r_{i,max}^l(z))^2)}{\lambda_i R_i^l(z)}} e^{-j \frac{2\pi}{\lambda_i} d_{i,m}^l(z)} e^{-jl\phi}, \quad (1)$$

where ϕ is the transverse azimuthal angle and l is the OAM mode number [38]; λ_i is the carrier wavelength; $\omega_i(z) = \omega_i \sqrt{1 + (\frac{z}{z_R})^2}$ is the beam spot of the fundamental Gaussian beam and ω_i is the beam waist radius; $z_R = \frac{\pi \omega_i^2}{\lambda_i}$ is the Rayleigh distance and we assume the same Rayleigh distance for all sub-systems; $R_i^l(z) = z \left[1 + \left(\frac{\pi \omega_i^2}{\lambda_i z} \right)^2 \right]$ is the curvature radius; $r_{i,max}^l(z) = \sqrt{\frac{|l|}{2}} \omega_i(z) = \omega_i \sqrt{\frac{|l|}{2} \left(1 + \left(\frac{z}{z_R} \right)^2 \right)}$ is the radius of maximum energy strength region, in which the channel response follows Frris law [6], [39], [40]; $d_{i,m}^l(z) = \sqrt{(r_{i,max}^l(z))^2 + z^2}$; $e^{-jl\phi}$ denotes the helical phase

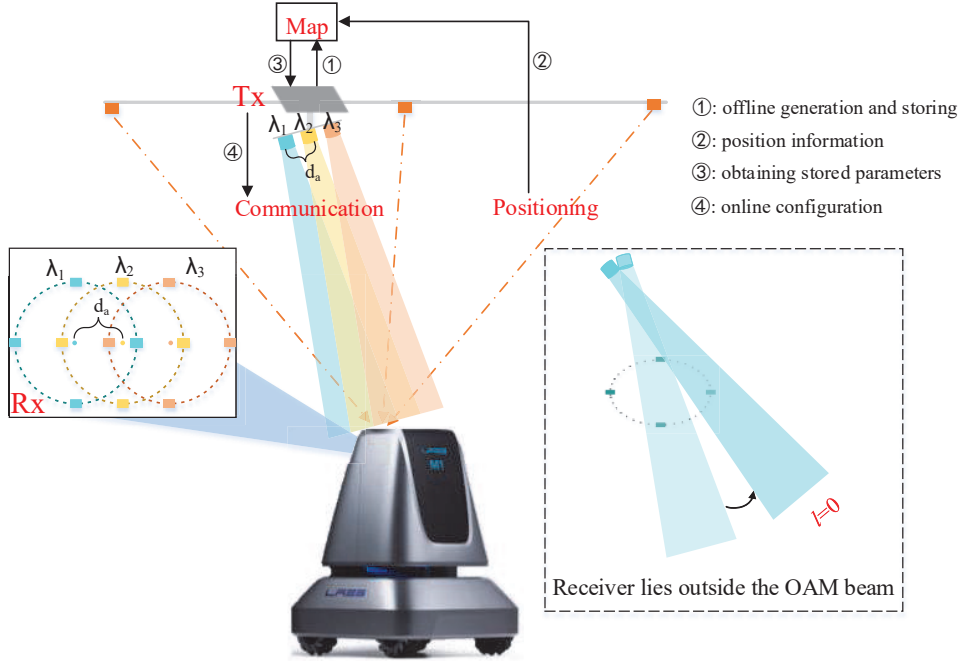


Fig. 1: The scenario of the intelligent terminal equipped with mmWave WDM and OAM system.

distribution of OAM wave with mode l and $l = 0$ for a plane wave; ζ_i^l incorporates both antenna gain and system loss of i -th sub-system with OAM mode l . Therefore, the link gain can be written as

$$g_i^l(r, z) = \frac{\zeta_i^l \lambda_i^2}{(4\pi)^2 (d_{i,m}^l(z))^2} \left(\frac{r}{r_{i,max}^l(z)} \right)^{2|l|} e^{\frac{2((r_{i,max}^l(z))^2 - r^2)}{\omega_i^2(z)}}. \quad (2)$$

According to Equation (1), the channel response can be represented as $h_i^l(r, \phi, z) = h_i^l(r, z)e^{-jl\phi}$. Due to inter-mode orthogonality, the OAM-based systems can coaxially transmit multiple OAM beams without inter-channel interference (ICI). We assume the same OAM modes employed in each sub-system, which can be perfectly separated at the receiver.

Figure 1 also gives the process of map-assisted method. The system solves optimization problems at all positions in an offline manner, quantifies these results into a few patterns, and then stores these results into a map. When obtaining the position information, the system looks up the parameters from the map, and configures the transmitter and receiver by adopting this parameters. In fact, if the system lies in the environment with lots of small-scale fading, the channel gain can not be determined even if the position of the transceiver is fixed. Therefore, the obtained map is not applicable in this scenario. However, in this paper, we mainly consider the mmWave frequency and short-range LOS environment, where the links are sparse and quasi-static. Apparently, both quantization error and positioning error will mismatch

the position with its optimal parameters, and thus lead to a performance loss. In the following chapters, we theoretically analyze the performance loss in two problems: power allocation and high dimensional constellation design, and find the features in maps by combining with numerical results.

III. POWER ALLOCATION MAP FOR MMWAVE WDM SYSTEMS

We consider the power allocation under short-range LOS communication scenario, and propose the concept of power allocation map for the proposed map-assisted approach.

A. Power Allocation Problem

We consider the power allocation to maximize the sum rate over all sub-channels, which is represented by

$$\begin{aligned} \max_{P_i^l} \quad & \sum_{i=1}^I \sum_{l \in \mathcal{L}} R_i^l(P_i^l) = \sum_{i=1}^I \sum_{l \in \mathcal{L}} \log_2 \left(1 + \frac{g_i^l P_i^l}{N_i} \right) \\ \text{s.t.} \quad & \sum_{i=1}^I \sum_{l \in \mathcal{L}} P_i^l = P_{sum}, \\ & P_i^l \geq 0, \quad l \in \mathcal{L}, i \in \mathcal{I} = \{1, 2, \dots, I\}, \end{aligned} \quad (3)$$

where \mathcal{L} denotes the set of OAM modes; P_i^l and N_i denote the allocated power and noise power, respectively; and P_{sum} denotes the total power of the transmitter.

Assume that the receiving antennas are placed on a circle of radius r_a . According to Section II, the system only adopts plane wave ($l = 0$) when the receiver lies outside the OAM beam, hence $\mathcal{L} = \{0\}$ in this situation. We treat plane wave as a special case and its features are also applicable to the mmWave WDM systems equipped with other kinds of non OAM antennas (such as array antennas) under short-range LOS link.

B. Power Allocation Map

We characterize the optimal power allocation according to the receiver location. We divide the space into regions and calculate the optimal power allocation of each region, assuming that the optimal power allocation of each region center can represent that in this region.

In general, the receiver moves in a three dimensional (3D) space. Since the link gain is independent of azimuth angle ϕ , the 3D map can be reduced due to rotational symmetry, such that we can only consider vertical distance z along the axis and horizontal distance r from the axis. As shown in Figure 2, the two dimensional (2D) map is an arbitrary cross-section of the OAM beam. The 2D map is divided into two regions, where region 1 is covered by the OAM beam and region 2 lies outside the OAM beam.

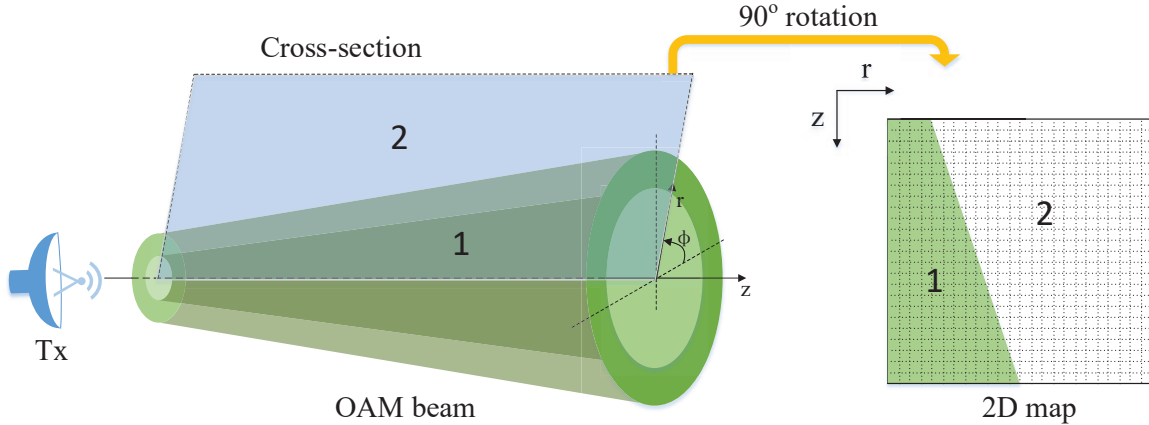


Fig. 2: The OAM transmission in the 3D space, and the arbitrary cross-section.

The power allocation map can be generated according to the 2D map and provide prior knowledge to configure the transceiver.

To reduce the demand of look-up table storing and searching in map-assisted method, we quantify the parameters into a small set, which means that the system employs approximate optimization to replace continuous optimization. More specifically, the system uses the optimal solution of one position as that of other positions, and all positions in the map will be classified into several categories. We adopt normalized sum-rate difference as the criterion when generating the power allocation map, where the power allocation of a position in a certain region is adopted to represent that of all positions in the region. The normalized sum-rate difference for position q_1 using the optimal power allocation of position q_2 can be expressed as

$$\begin{aligned} \Delta \bar{R}(q_1, q_2) &\triangleq \left| 1 - \frac{\sum_{i=1}^I \sum_{l \in \mathcal{L}} R_i^{l,(q_2)}(P_i^{l,(q_1)})}{\sum_{i=1}^I \sum_{l \in \mathcal{L}} R_i^{l,(q_2)}(P_i^{l,(q_2)})} \right| \\ &= \left| 1 - \frac{\sum_{i=1}^I \sum_{l \in \mathcal{L}} \log_2 \left(1 + \frac{g_i^{l,(q_2)} P_i^{l,(q_1)}}{N_i} \right)}{\sum_{i=1}^I \sum_{l \in \mathcal{L}} \log_2 \left(1 + \frac{g_i^{l,(q_2)} P_i^{l,(q_2)}}{N_i} \right)} \right|, \quad (4) \end{aligned}$$

where $P_i^{l,(q_1)}$ and $P_i^{l,(q_2)}$ are the optimal powers of the l -th OAM mode in the i -th sub-system at the positions q_1 and q_2 , respectively; $g_i^{l,(q_2)}$ is the link gain of the l -th OAM mode in the i -th sub-system at position q_2 ; and N_i is the power of additive white Gaussian noise (AWGN) that only depends on system bandwidth in the i -th sub-system.

We adopt clustering approach to quantify the parameters of all positions with a distortion threshold τ_s . Letting \mathcal{Q} denote the set of all positions, we randomly select a position q_a from \mathcal{Q} with the optimal power allocation $\mathbf{p}^{(q_a)}$. For other positions, if the normalized sum-rate differences from $\mathbf{p}^{(q_a)}$ is lower than threshold τ_s , we classify these positions and q_a into one category and remove these positions from

\mathcal{Q} . Moreover, the power allocation of this category is set to be $\mathbf{p}^{(q_a)}$. Repeat the random position selection and classification until all positions are classified into certain categories. Then, we store the generated power allocation map and calculate the normalized sum-rate difference $\Delta\bar{R}_s$, which is the summation of the normalized sum-rate differences at all positions. We repeat the whole above process C_r times and select the map with lowest $\Delta\bar{R}_s$ as the final power allocation map \mathcal{P}_{map} . In this paper, we set $\tau_s = 0.02$ and $C_r = 100$.

C. Rate-difference Analysis on Power Allocation Map

1) *Sum-rate Difference for the Regions Outside the OAM Beam* : We first investigate the features of plane wave only regions ($\mathcal{L} = \{0\}$), and for any two sub-channels i and j , we have

$$\frac{g_i^{(2)}}{g_i^{(1)}} = \frac{g_j^{(2)}}{g_j^{(1)}} = \frac{(d_{i,m}^{0,(1)}(z))^2}{(d_{i,m}^{0,(2)}(z))^2} = \frac{(z^{(1)})^2}{(z^{(2)})^2}, \quad (5)$$

where $d_{i,m}^{0,(1)}(z)$ and $d_{i,m}^{0,(2)}(z)$ are the transmission distances at the positions 1 and 2, respectively, and $d_{i,m}^0(z) = z$ since the beam axis aligns with one of the receiving antennas in each sub-channel. Equation (5) implies that the link gain variations in different sub-channels are only related to the distance. We denote $K \triangleq \frac{g_i^{(2)}}{g_i^{(1)}}$ represent the variation of link gains in the i -th sub-channel from position 1 to position 2. We first assume high SNRs in each sub-channel due to short-range LOS link, such that the allocated power of each sub-channel is positive. Thus, by employing Karush-Kuhn-Tucker (KKT) method in Equation (3), the allocated power of i -th sub-channel can be written as $P_i^* = \frac{1}{\mu} - \frac{N_i}{g_i}$, where μ is a Lagrange multiplier and satisfies $\frac{I}{\mu} = P_{sum} + \sum_{j=1}^I \frac{N_j}{g_j}$. Hence, we have

$$P_i^* = \frac{P_{sum}}{I} + \frac{1}{I} \sum_{j=1}^I \frac{N_j}{g_j} - \frac{N_i}{g_i}, \quad i \in \mathcal{I} = \{1, 2, \dots, I\}. \quad (6)$$

Based on the link gain with $l = 0$ in Equation (2), we have

$$\frac{N_i}{g_i} = \frac{(\zeta)_1 N_i}{(\zeta)_i N_1} \cdot \frac{\lambda_1^2}{\lambda_i^2} \cdot \frac{N_1}{g_1} = \xi_i \cdot \frac{\lambda_1^2}{\lambda_i^2} \cdot \frac{N_1}{g_1}. \quad (7)$$

Equation (7) implies that $\frac{N_i}{g_i}$ in each sub-channel i can be represented by $\frac{N_1}{g_1}$. And we can note that $P_i^{*(1)} = \frac{P_{sum}}{I} + \frac{\lambda_i^2 N_1}{g_1^{(1)}} \left(\frac{1}{I} \sum_{j=1}^I \frac{\xi_j}{\lambda_j^2} - \frac{\xi_i}{\lambda_i^2} \right)$ and $P_i^{*(2)} = \frac{P_{sum}}{I} + \frac{\lambda_i^2 N_1}{K g_1^{(1)}} \left(\frac{1}{I} \sum_{j=1}^I \frac{\xi_j}{\lambda_j^2} - \frac{\xi_i}{\lambda_i^2} \right)$ are the optimal power allocations of position 1 and position 2, respectively. Assuming that at position 2, the mmWave WDM system still adopts the optimal power allocation of position 1, the rate difference of the i -th sub-channel can be expressed as

$$\Delta R_i = \log_2 \left(1 + \frac{g_i^{(2)} P_i^{*(2)}}{N_i} \right) - \log_2 \left(1 + \frac{g_i^{(2)} P_i^{*(1)}}{N_i} \right), \quad (8)$$

and the sum-rate difference is given by

$$\Delta R = \sum_{i=1}^I \Delta R_i = -\log_2 \prod_{i=1}^I \left[1 + \frac{\frac{\lambda_1^2 N_1}{g_1^{(1)}} (K-1) \left(\sum_{j=1}^I \frac{\xi_j}{\lambda_j^2} - \frac{I \xi_i}{\lambda_i^2} \right)}{K P_{sum} + \frac{\lambda_1^2 N_1}{g_1^{(1)}} \sum_{j=1}^I \frac{\xi_j}{\lambda_j^2}} \right]. \quad (9)$$

We have the following result.

Theorem 1. For $K > 1$, $\frac{\partial \Delta R}{\partial K} > 0$ always holds and an upper bound independent of K can be given as

$$\Delta R \leq \lim_{K \rightarrow \infty} \Delta R = -\log_2 \prod_{i=1}^I \left[1 + \frac{\frac{\lambda_1^2 N_1}{g_1^{(1)}} \left(\sum_{j=1}^I \frac{\xi_j}{\lambda_j^2} - \frac{I \xi_i}{\lambda_i^2} \right)}{P_{sum}} \right]. \quad (10)$$

Moreover, $\frac{\partial^2 \Delta R}{\partial K^2} < 0$ always holds within range $K > K_{0,ub}$, where $K_{0,ub}$ is close to 1 under high SNR regime and can be calculated by

$$K_{0,ub} = \max_i \left\{ \frac{\frac{\lambda_1^2 N_1}{g_1^{(1)}} \left[\frac{1}{4} \sum_{j=1}^I \frac{\xi_j}{\lambda_j^2} + \sqrt{\frac{9}{16} + \frac{\lambda_1^2 N_1}{2g_1^{(1)} P_{sum}} \left(\sum_{j=1}^I \frac{\xi_j}{\lambda_j^2} - \frac{I \xi_i}{\lambda_i^2} \right) \sum_{j=1}^I \frac{\xi_j}{\lambda_j^2} - \frac{I \xi_i}{\lambda_i^2} \right]}{\frac{\lambda_1^2 N_1}{g_1^{(1)}} \left(\sum_{j=1}^I \frac{\xi_j}{\lambda_j^2} - \frac{I \xi_i}{\lambda_i^2} \right) + \left[\frac{3}{4} - \sqrt{\frac{9}{16} + \frac{\lambda_1^2 N_1}{2g_1^{(1)} P_{sum}} \left(\sum_{j=1}^I \frac{\xi_j}{\lambda_j^2} - \frac{I \xi_i}{\lambda_i^2} \right) \right] P_{sum}} \right\}. \quad (11)$$

Proof. See Appendix A. □

According to Theorem 1, as $\frac{\partial^2 \Delta R}{\partial K^2} < 0$ within range $K > K_{0,ub}$ and $K_{0,ub}$ is close to 1, the sum-rate difference ΔR converges to the upper bound for sufficiently large K . When the channel condition deteriorates, namely $K < 1$, we still follow similar approach. Let K_{min} satisfy $\frac{K_{min} g_1^{(1)}}{N_1} = \left(\frac{g_1}{N_1} \right)_{min} \triangleq \frac{I \cdot \max_i \left(\frac{\xi_i \lambda_1^2}{\lambda_i^2} \right) - \sum_{j=1}^I \frac{\xi_j \lambda_1^2}{\lambda_j^2}}{P_{sum}}$, where $\left(\frac{g_1}{N_1} \right)_{min}$ is the lowest link gain over noise power for the first sub-channel ensuring positive allocated power in each sub-channel. If $0 < K < K_{min}$, the allocated power in each sub-channel no longer satisfies Equation (6) and can be obtained by traditional water-filling algorithm. Although, it is difficult to get the closed-form solution of the sum-rate difference, we still have the following result on the upper bound.

Theorem 2. When $0 < K < 1$, sum-rate difference ΔR satisfies

$$\begin{aligned} \Delta R &\leq \Delta \dot{R} \triangleq -\log_2 \prod_{i=1}^I \left[1 + \frac{\frac{\lambda_1^2 N_1}{g_1^{(1)}} (K-1) \left(\sum_{j=1}^I \frac{\xi_j}{\lambda_j^2} - \frac{I \xi_i}{\lambda_i^2} \right)}{K P_{sum} + \frac{\lambda_1^2 N_1}{g_1^{(1)}} \sum_{j=1}^I \frac{\xi_j}{\lambda_j^2}} \right] \\ &\leq \Delta \dot{R}^u \triangleq \log_2 \prod_{i=1}^I \left(\frac{\lambda_i^2}{\xi_i} \right) + I \log_2 \left(\frac{1}{I} \sum_{j=1}^I \frac{\xi_j}{\lambda_j^2} \right), \end{aligned} \quad (12)$$

and $\frac{\Delta \dot{R}}{\partial K} < 0$. Moreover, within range $K_{min} < K < 1$, ΔR satisfies $\Delta R = \Delta \dot{R}$, $\frac{\partial^2 \Delta R}{\partial K^2} > 0$ and $\frac{\partial^3 \Delta R}{\partial K^3} < 0$.

Proof. See Appendix B. □

According to Equations (9) and (36), it is easily obtained that $\lim_{k \rightarrow 1^-} \Delta R = 0$ and $\lim_{k \rightarrow 1^-} \frac{\Delta R}{\partial K} = 0$. Based on Theorem 2, as $\frac{\partial^3 \Delta R}{\partial K^3} < 0$ and $\frac{\partial^2 \Delta R}{\partial K^2} > 0$ within $K_{min} < K < 1$, the increment slope of $\frac{\partial \Delta R}{\partial K}$ within range $[K_{min}, 1]$ decreases as K increases. Meanwhile, since $\frac{\Delta R}{\partial K} < 0$ and $\lim_{K \rightarrow 1^-} \frac{\Delta R}{\partial K} = 0$ within $K_{min} < K < 1$, the decrement slope of ΔR tends to 0 as K approaches one. Moreover, ΔR converges to 0 as K increases to 1 according to $\lim_{k \rightarrow 1^-} \Delta R = 0$. Given sum-rate difference tolerance ϵ satisfying $0 < \epsilon < \Delta \dot{R}^u$, $\Delta R < \epsilon$ always holds within range $K_\epsilon < K < 1$, where $K_\epsilon = \Delta \dot{R}^{-1}(\epsilon)$ is the inverse function of $\Delta \dot{R}$ within range $0 < K < 1$. For $\epsilon \geq \Delta \dot{R}^u$, we can set $K_\epsilon = 0$, which indicates that for range $0 < K < 1$, $\Delta R < \epsilon$ always holds.

Next, we investigate the effect of $\frac{g_1^{(1)}}{N_1}$ on the sum-rate difference. To facilitate the analysis, we provide the following lemma.

Lemma 1. For a_1, a_2, \dots, a_n and b_1, b_2, \dots, b_n that satisfy $\sum_{i=1}^n b_i = 0$, $a_i b_i \geq 0$, and $a_i + b_i > -1$, we have

$$\prod_{i=1}^n (1 + a_i + b_i) \leq \prod_{i=1}^n (1 + a_i). \quad (13)$$

Proof. See Appendix C. □

Then, we have the following result.

Theorem 3. The upper bound independent of K decreases as $\frac{g_1^{(1)}}{N_1}$ increases within range $K > 1$. The upper bound $\Delta \dot{R}$ also decreases as $\frac{g_1^{(1)}}{N_1}$ increases within range $0 < K < 1$, and for any given ϵ satisfying $0 < \epsilon < \Delta \dot{R}^u$, range $\Delta \dot{R} < \epsilon$ expands as $\frac{g_1^{(1)}}{N_1}$ increases.

Proof. See Appendix D. □

Theorem 3 implies that under larger SNR regime, the system can use fixed power allocation over a wider range of channel variation. Given sum-rate difference tolerance ϵ , we adopt fixed power allocation generated from the channel condition satisfying $\frac{g_1^{(1)}}{N_1} \geq U_p^{-1}(\epsilon)$, where U_p^{-1} is the inverse function of the upper bound in Equation (10). The sum-rate difference is always lower than ϵ within range $K > K_\epsilon$.

We present numerical results on the properties of plane wave-based mmWave WDM in short-distance LOS environment. We set the number of sub-channels $I = 10$, $P_{sum} = 1$. Assume that the carrier frequency of the first sub-channel is $f_1 = 60\text{GHz}$ and the carrier frequency interval between two adjacent sub-channels is $\Delta f = 1\text{GHz}$. Further assume that parameter ζ and the noise powers of all sub-channels are the same, i.e., $\xi_1 = \xi_2 = \dots = \xi_I = 1$.

Figure 3 shows the sum-rate differences of mmWave WDM systems within $K > 1$. It is seen that in both values of $\frac{g_1^{(1)}}{N_1}$, the two sum-rate differences increase with K . Comparing Figure 3a with Figure 3b,

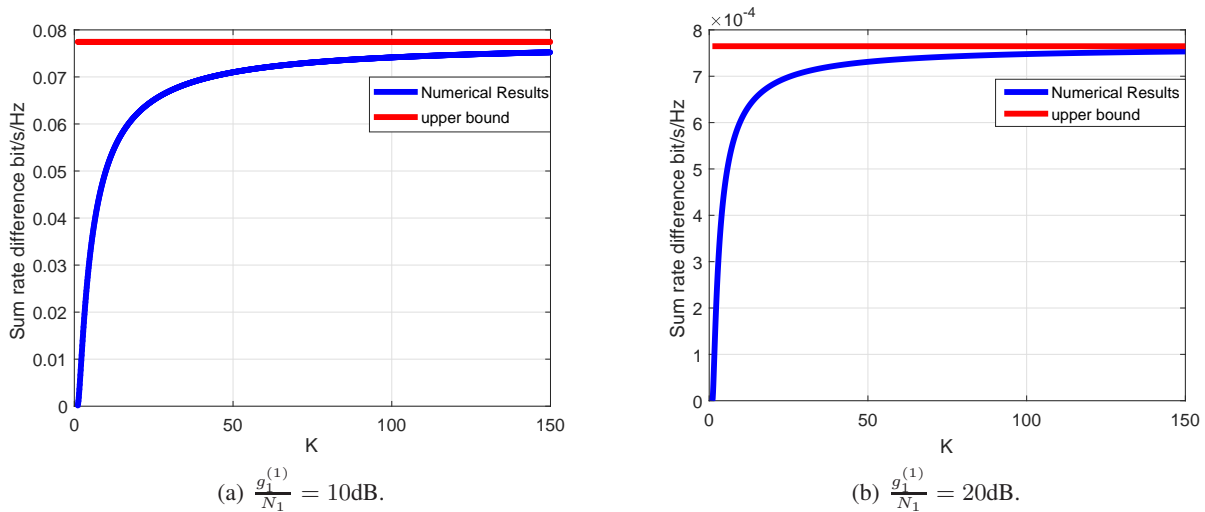


Fig. 3: The sum-rate difference of $K > 1$.

it is seen that larger $\frac{g_1^{(1)}}{N_1}$ can lead to lower gap and lower upper bound. The reason is that for high $\frac{g_1^{(1)}}{N_1}$, the optimal power allocation keeps almost unchanged for large K .

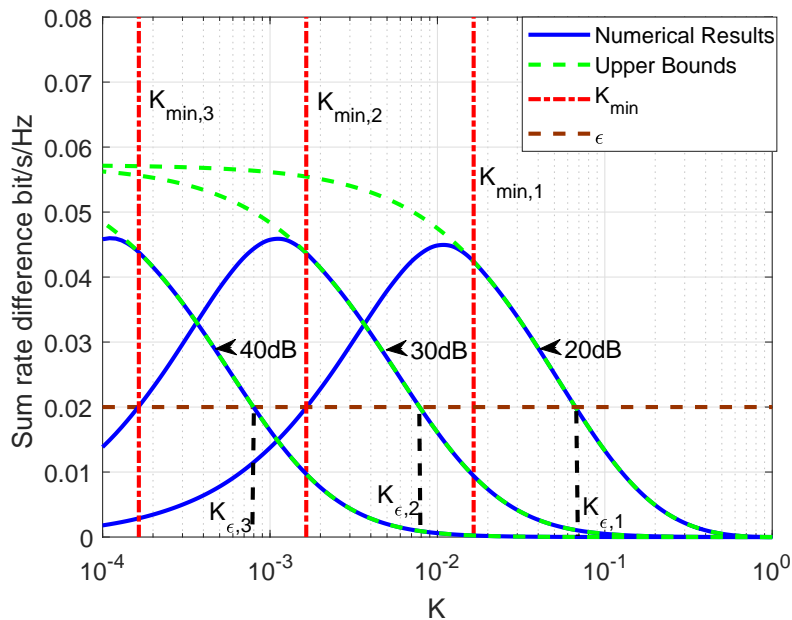


Fig. 4: The sum-rate difference of $0 < K < 1$.

Figure 4 gives the sum-rate differences of mmWave WDM systems within $0 < K < 1$, wherein upper bounds stand for $\Delta \hat{R}$. Three cases have been considered, i.e., $\frac{g_1^{(1)}}{N_1} = \varpi_i$, $i = \{1, 2, 3\}$, where

$\varpi_1 = 20\text{dB}$, $\varpi_2 = 30\text{dB}$ and $\varpi_3 = 40\text{dB}$. Let $K_{\min,i} = (\frac{g_i}{N_i})_{\min}/10^{\frac{\varpi_i}{10}}$ and $K_{\epsilon,i} = \Delta\hat{R}_i^{-1}(\epsilon)$ for $i = \{1, 2, 3\}$. It is seen that $K_{\epsilon,3} < K_{\epsilon,2} < K_{\epsilon,1}$ for $\epsilon = 0.02$, which indicates that larger $\frac{g_i^{(1)}}{N_i}$ can lead to a wider range of $\Delta R < \epsilon$. The reason is that as $\frac{g_i^{(1)}}{N_i}$ increases, the change of power allocation decreases for any K . Meanwhile, the numerical results of ΔR are always lower than upper bounds $\Delta\hat{R}$ within $0 < K < K_{\min}$ and equal to $\Delta\hat{R}$ within $K_{\min} < K < 1$. We can observed that the gap between numerical results and upper bounds increases as K decreases. Within this range, the upper bound $\Delta\hat{R}$ difficultly fits the sum-rate difference, and thus only numerical results can be adopted in reality.

2) *The Region Inside the OAM Beam:* We focus on the link gain ratios within OAM beam regions, where \mathcal{L} consists of several OAM modes. Assume that $\lambda_i > \lambda_j$ and $|l_1| > |l_2|$. Denote λ_a as an arbitrary carrier wavelength. Let $r = \beta r_{a,\max}^{l_m}(z)$, where β is a non-negative number and l_m is an arbitrary nonzero OAM mode. It is seen that when λ_a and l_m are fixed, radius r can be replaced by β , which indicates that β can determine the horizontal distance from the beam axis. Denoting $a_{i,j}^l(\beta, z) \triangleq \frac{g_i^l(\beta r_{a,\max}^{l_m}(z), z) \cdot N_j}{g_j^l(\beta r_{a,\max}^{l_m}(z), z) \cdot N_i}$ for $1 \leq i, j \leq I$, we have

$$a_{i,j}^l(\beta, z) = \frac{\zeta_i^l N_j}{\zeta_j^l N_i} \left(\frac{\lambda_j}{\lambda_i} \right)^{|l|-2} \frac{\omega_j^2 \frac{|l|}{2} \left(1 + \frac{z^2}{z_R^2} \right) + z^2}{\omega_i^2 \frac{|l|}{2} \left(1 + \frac{z^2}{z_R^2} \right) + z^2} e^{\beta^2 |l_m| \left(\frac{\lambda_i}{\lambda_j} - 1 \right)}. \quad (14)$$

Note that term $\frac{\omega_j^2 \frac{|l|}{2} \left(1 + \frac{z^2}{z_R^2} \right) + z^2}{\omega_i^2 \frac{|l|}{2} \left(1 + \frac{z^2}{z_R^2} \right) + z^2}$ increases monotonically with z when $\lambda_i > \lambda_j$ and converges to 1. Moreover, this term converges rapidly because $\omega^2 = z_R \lambda / \pi \ll 1$ in short-range mmWave systems. For instance, considering that $l = 2$, $z_R = 4\text{m}$ and two carrier frequencies $f_i = 60\text{GHz}$ and $f_j = 65\text{GHz}$, this term is larger than 0.995 for $z > 0.1\text{m}$. Hence, the above link gain ratio can be approximated as $a_{i,j}^l(\beta, z) \approx \frac{\zeta_i^l N_j}{\zeta_j^l N_i} \left(\frac{\lambda_j}{\lambda_i} \right)^{|l|-2} e^{\beta^2 |l_m| \left(\frac{\lambda_i}{\lambda_j} - 1 \right)}$. Then, denoting $a_i^{l_1, l_2}(\beta, z) \triangleq \frac{g_i^{l_1}(\beta r_{a,\max}^{l_m}(z), z)}{g_i^{l_2}(\beta r_{a,\max}^{l_m}(z), z)}$ for $l_1, l_2 \in \mathcal{L}$, and $|l_1|, |l_2|$ not very large, we have

$$\begin{aligned} a_i^{l_1, l_2}(\beta, z) &= \frac{\zeta_i^{l_1}}{\zeta_i^{l_2}} \left(\frac{\lambda_a}{\lambda_i} \right)^{|l_1| - |l_2|} \frac{\omega_i^2 \frac{|l_2|}{2} \left(1 + \frac{z^2}{z_R^2} \right) + z^2}{\omega_i^2 \frac{|l_1|}{2} \left(1 + \frac{z^2}{z_R^2} \right) + z^2} (\beta^2 |l_m|)^{|l_1| - |l_2|} \frac{|l_2|^{|l_2|}}{|l_1|^{|l_1|}} e^{|l_1| - |l_2|} \\ &\approx \frac{\zeta_i^{l_1}}{\zeta_i^{l_2}} \left(\frac{\lambda_a}{\lambda_i} \right)^{|l_1| - |l_2|} (\beta^2 |l_m|)^{|l_1| - |l_2|} \frac{|l_2|^{|l_2|}}{|l_1|^{|l_1|}} e^{|l_1| - |l_2|}. \end{aligned} \quad (15)$$

Considering link gain ratios at different positions, we have the following on the ratios

$$\begin{aligned} \frac{a_{i,j}^{l_1, (1)}}{a_{i,j}^{l_1, (2)}} &= \frac{a_{i,j}^{l_1}(\beta_1, z_1)}{a_{i,j}^{l_1}(\beta_2, z_2)} = e^{|l_m| \left(\frac{\lambda_i}{\lambda_j} - 1 \right) (\beta_1^2 - \beta_2^2)}, \\ \frac{a_i^{l_1, l_2, (1)}}{a_i^{l_1, l_2, (2)}} &= \frac{a_i^{l_1, l_2}(\beta_1, z_1)}{a_i^{l_1, l_2}(\beta_2, z_2)} = \left(\frac{\beta_1}{\beta_2} \right)^{2(|l_1| - |l_2|)}. \end{aligned} \quad (16)$$

According to Equation (16), the link gain ratios are primarily determined by β_1 and β_2 , and are both equal to 1 if $\beta_1 = \beta_2$. This indicates that for the positions with the same β , $a_{i,j}^l$ and $a_i^{l_1, l_2}$ remain

unchanged, i.e., all sub-channels have uniform link gain ratio. Assume that the mmWave WDM system at positions 1 and 2 ($\beta_1 = \beta_2$) activates¹ the same sub-channels $\{\mathcal{L}_1 \cup \mathcal{L}_2 \cup \dots \cup \mathcal{L}_I\}$, where \mathcal{L}_i , $1 \leq i \leq I$ is the set of activated OAM modes in the i -th sub-system. Denote $L_i = |\mathcal{L}_i|$ as the number of activated OAM modes in the i -th sub-system and $N_a \triangleq \sum_{i=1}^I L_i$. Considering that this system adopts the optimal power allocation of position 1 at position 2, the sum-rate difference can be given by

$$\Delta R = - \sum_{i=1}^I \sum_{\tilde{l} \in \mathcal{L}_i} \log_2 \left[1 + \frac{(K-1) \left(\sum_{j=1}^I \sum_{l \in \mathcal{L}_j} \frac{a_{1,j}^{l,(1)} N_1}{g_1^{l,(1)}} - N_a \frac{a_{1,i}^{\tilde{l},(1)} N_1}{g_1^{\tilde{l},(1)}} \right)}{K P_{sum} + \sum_{j=1}^I \sum_{l \in \mathcal{L}_j} \frac{a_{1,j}^{l,(1)} N_1}{g_1^{l,(1)}}} \right], \quad (17)$$

where $K = \frac{g_i^{l,(2)}}{g_i^{l,(1)}}$ for $1 \leq i \leq I, l \in \mathcal{L}_i$. It is seen that the above form of sum-rate difference is similar to that in Equation (9). Therefore, we have the following result.

Theorem 4. *Given λ_a and l_m , and letting $r = \beta r_{a,max}^{l_m}(z)$, the link gain ratio between any two sub-channels remains approximately unchanged for any z in OAM beam regions, under the same β . Moreover, if the system activates the same sub-channels at these positions, the sum-rate difference in Equation (17) has the following upper bound independent of K ,*

$$\Delta R \leq \lim_{K \rightarrow \infty} \Delta R = - \sum_{i=1}^I \sum_{\tilde{l} \in \mathcal{L}_i} \log_2 \left(1 + \frac{\sum_{j=1}^I \sum_{l \in \mathcal{L}_j} \frac{a_{1,j}^{l,(1)} N_1}{g_1^{l,(1)}} - N_a \frac{a_{1,i}^{\tilde{l},(1)} N_1}{g_1^{\tilde{l},(1)}}}{P_{sum}} \right), \quad (18)$$

and satisfies $\frac{\partial \Delta R}{\partial K} < 0$, $\frac{\partial^2 \Delta R}{\partial K^2} > 0$ and $\frac{\partial^3 \Delta R}{\partial K^3} < 0$ for $K_{min}^o < K < 1$, where K_{min}^o is the boundary condition on activating the same sub-channels.

Proof. The proof is similar to that in Theorems 1 and 2, and is thus omitted here. \square

Here, we present numerical results on the upper bound in Equation (18). We set $I = 5$, $\Delta f = 1\text{GHz}$ and $\mathcal{L} = \{0, -1, +1\}$. We consider that the vertical distance z of position 1 is 3m and the z of position 2 changes from 0.3m to 3m. Since the link gain variations of all sub-channels are the same for the positions with a fixed β , we can still adopt K to represent these link gain variations.

From Figure 5, it is seen that the sum-rate difference in each sub-figure converges to the upper bound as K increases, and the trends are similar to those in the region outside OAM beam (shown in Figure 3). This indicates that the sum-rate difference feature at the positions with same β is similar to that in the region outside OAM beam and thus the conclusions in Section III-C1 are also applied to the OAM beam region.

Then, we consider the sum-rate differences at positions with different β . Assume that the system activates the same sub-channels at positions $q = \{0, 1, 2\}$, where the corresponding coordinates are

¹If a sub-channel has non-zero power, we say that the system activates this sub-channel.

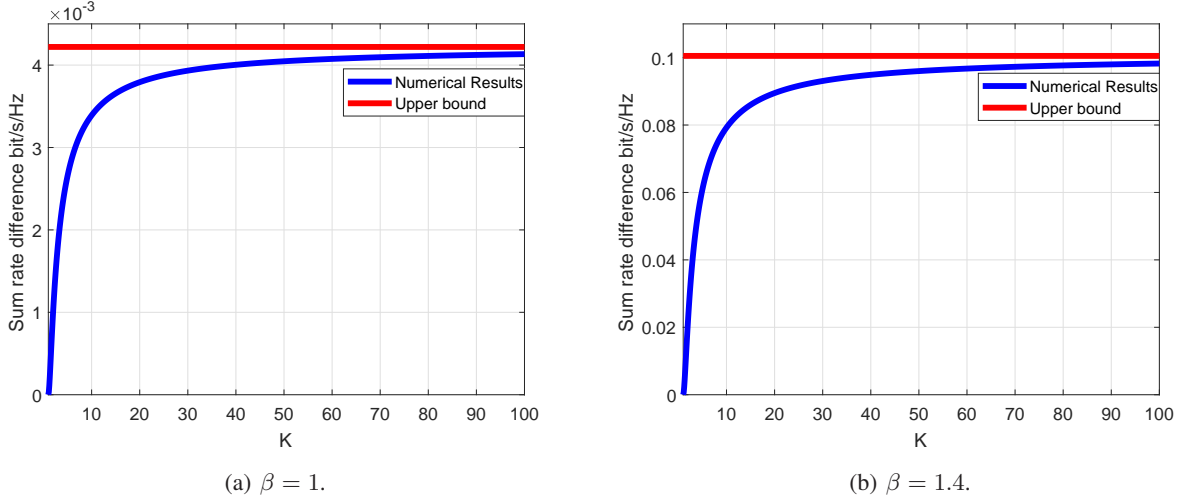


Fig. 5: The sum-rate difference and the upper bound in Equation (18).

$(\beta_q r_{a,max}^{lm}(z_q), z_q)$. Assuming that $z_0 = z_1$ and $\beta_1 = \beta_2$, the sum-rate difference at position 2 using the optimal power allocation of position 0 can be written as

$$\Delta R = - \sum_{i=1}^I \sum_{\tilde{l} \in \mathcal{L}_i} \log_2 \left[1 + \frac{\sum_{j=1}^I \sum_{l \in \mathcal{L}_j} \left(\frac{N_j}{g_j^{l,(1)}} - \frac{N_j}{g_j^{l,(2)}} \right) + N_a \left(\frac{N_i}{g_i^{l,(2)}} - \frac{N_i}{g_i^{l,(1)}} \right) + N_a \Delta P_i^{\tilde{l}}}{P_{sum} + \sum_{j=1}^I \sum_{l \in \mathcal{L}_j} \frac{N_j}{g_j^{l,(2)}}} \right], \quad (19)$$

where $\Delta P_i^{\tilde{l}} \triangleq \frac{1}{N_a} \sum_{j=1}^I \sum_{l \in \mathcal{L}_j} \left(\frac{N_j}{g_j^{l,(0)}} - \frac{N_j}{g_j^{l,(1)}} \right) + \left(\frac{N_i}{g_i^{l,(1)}} - \frac{N_i}{g_i^{l,(0)}} \right)$ is the optimal power allocation difference of the i -th wavelength with OAM mode \tilde{l} between positions 0 and 1. In general, $\frac{N_i}{g_i^{l,(1)}}$, $1 \leq i \leq I, l \in \mathcal{L}_i$ of the activated sub-channels are very small compared with P_{sum} in short-range LOS environment, and the sum-rate difference in Equation (19) can be approximated as

$$\begin{aligned} \Delta R \approx & - \sum_{i=1}^I \sum_{\tilde{l} \in \mathcal{L}_i} \log_2 \left[1 + \frac{(K-1) \left(\sum_{j=1}^I \sum_{l \in \mathcal{L}_j} \frac{a_{1,j}^{l,(1)} N_1}{g_1^{l,(1)}} - N_a \frac{a_{1,i}^{\tilde{l},(1)} N_1}{g_1^{l,(1)}} \right)}{K P_{sum} + \sum_{j=1}^I \sum_{l \in \mathcal{L}_j} \frac{a_{1,j}^{l,(1)} N_1}{g_1^{l,(1)}}} \right] \\ & - \sum_{i=1}^I \sum_{\tilde{l} \in \mathcal{L}_i} \frac{N_a \log_2 e \cdot \Delta P_i^{\tilde{l}}}{P_{sum} + \sum_{j=1}^I \sum_{l \in \mathcal{L}_j} \frac{N_j}{g_j^{l,(1)}} + N_a \left(\frac{N_i}{g_i^{l,(2)}} - \frac{N_i}{g_i^{l,(1)}} \right)}. \end{aligned} \quad (20)$$

Denoting

$$\ddot{a}_i^l \triangleq \frac{g_i^l(\beta_0 r_{a,max}^{lm}(z_0), z_0)}{g_i^l(\beta_1 r_{a,max}^{lm}(z_1), z_1)} = \left(\frac{\beta_0}{\beta_2} \right)^{2|l|} e^{l_m |(\beta_2^2 - \beta_0^2)| \left(\frac{\lambda_a}{\lambda_i} \right)}, \quad (21)$$

we have

$$\left| \Delta P_i^{\tilde{l}} \right| = \left| \sum_{j=1}^I \sum_{l \in \mathcal{L}_j} (1 - \ddot{a}_j^l) \frac{N_j}{g_j^{l,(0)}} - N_a (1 - \ddot{a}_i^{\tilde{l}}) \frac{N_i}{g_i^{l,(0)}} \right|$$

$$\leq \sum_{j=1}^I \sum_{l \in \mathcal{L}_j} \left| 1 - \bar{a}_j^l \right| \frac{N_j}{g_j^{l,(0)}} + N_a \left| 1 - \bar{a}_i^l \right| \frac{N_i}{g_i^{l,(0)}}. \quad (22)$$

Then, the sum-rate difference at position 2 using the optimal power allocation of position 0 can be approximated as

$$\Delta R \approx - \sum_{i=1}^I \sum_{\bar{l} \in \mathcal{L}_i} \log_2 \left[1 + \frac{(K-1) \left(\sum_{j=1}^I \sum_{l \in \mathcal{L}_j} \frac{a_{1,j}^{l,(1)} N_1}{g_1^{l,(1)}} - N_a \frac{a_{1,i}^{\bar{l},(1)} N_1}{g_1^{\bar{l},(1)}} \right)}{K P_{sum} + \sum_{j=1}^I \sum_{l \in \mathcal{L}_j} \frac{a_{1,j}^{l,(1)} N_1}{g_1^{l,(1)}}} \right], \quad (23)$$

provided that β_2 is sufficiently close to β_0 or all link status $\frac{g_i^{l,(0)}}{N_i}, l \in \mathcal{L}_i, 1 \leq i \leq I$ are sufficiently high.

When β_2 is sufficiently close to β_0 , positions 0 and 1 can be regarded as one position. Moreover, when all link status $\frac{g_i^{l,(0)}}{N_i}, l \in \mathcal{L}_i, 1 \leq i \leq I$ are sufficiently high, the power allocation difference between position 0 and position 1 in each sub-channel is very small. Under the above two conditions, the sum-rate difference at position 2 using the optimal power allocation of position 0 is close to that using the optimal power allocation of position 1, which is the same as the situation in Theorem 4. Moreover, since the sum-rate difference in Theorem 4 has the similar features to the sum-rate difference in the region outside OAM beam, we can know that the system can employ a fixed power allocation in the OAM beam region with high SNR.

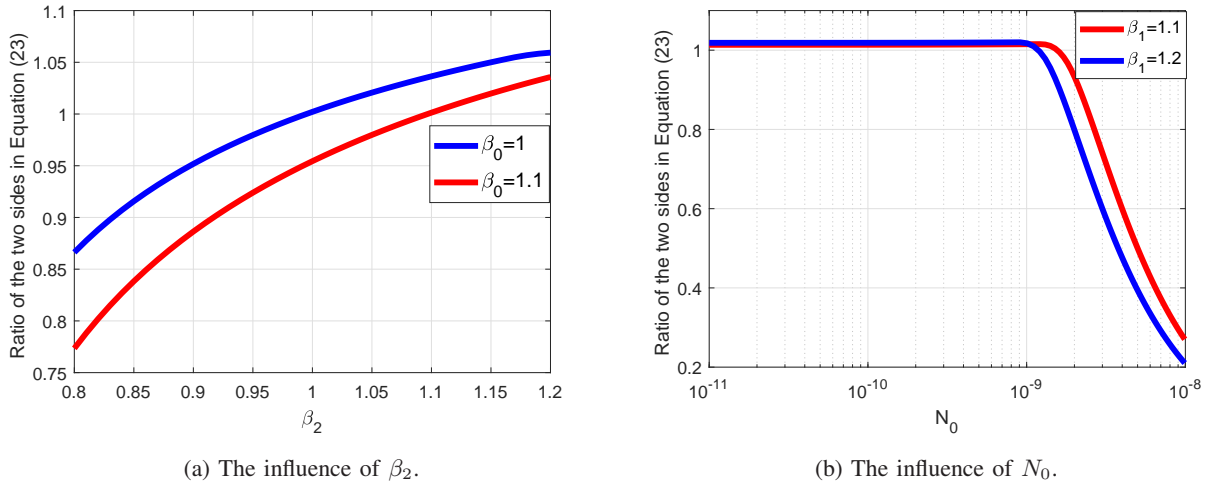


Fig. 6: The ratio of ΔR to its approximation in Equation (23).

Figure 6 gives some examples on the ratio of ΔR to its approximation in Equation (23). The system parameters are the same to those in Figure 5. We consider that $z_0 = 0.5m$ and $z_2 = 4m$. In Figure 6b, we fix the links gain $g_i^{l,(0)}, l \in \mathcal{L}_i, 1 \leq i \leq I$, and change the noise variance N_0 . Assume that $N_i = N_0, 1 \leq i \leq I$. From Figure 6a, we know that the ratio is close to 1 when β_2 is sufficiently close to

β_0 . From Figure 6b, we know that the ratio is close to 1 when N_0 is small, i.e., $\frac{g_i^{l,(0)}}{N_i}, l \in \mathcal{L}_i, 1 \leq i \leq I$ is high. The above results verify our analysis and show the validity of the approximation in Equation (23).

D. Category for Power Allocation Map

Based on the concept of using approximate optimization to replace continuous optimization, we consider that the system adopts one power allocation pattern in each category. Since that it is difficult to obtain an accurate position variation range when given a sum-rate difference tolerance, we attempt to qualitatively analyze the classification in power allocation map based on the results of the above subsection.

1) *Very Few Categories Outside the OAM Beam Region:* From the analysis of sum-rate difference outside the OAM beam region (cf. Section III-C1), for any ϵ , the system can use fixed power allocation within range $K > K_\epsilon$, provided $\frac{g_i^{(1)}}{N_i} \geq U_p^{-1}(\epsilon)$. According to Equation (4), the normalized sum-rate difference can be re-expressed as $\Delta \bar{R}(q_1, q_2) = \Delta R/R^{(q_2)}$, where $R^{(q_2)} \triangleq \sum_{i=1}^I \sum_{l \in \mathcal{L}} \log_2 \left(1 + g_i^{l,(q_2)} P_i^{l,(q_2)} / N_i \right)$. For a given threshold τ_s , we can get $\epsilon = \tau_s R^{(q_2)}$, which implies that positions q_1 and q_2 can be classified into one category if the sum-rate difference ΔR at position q_2 is lower than ϵ . Since the link gains of all sub-channels are very large for short-range LOS links, $R^{(q_2)}$ can be very large, and thus ϵ is also very large. According to Theorem 3, $U_p^{-1}(\epsilon)$ decreases as ϵ increases, and thus $U_p^{-1}(\epsilon)$ can be very small. This implies that $\frac{g_i^{(1)}}{N_i} \geq U_p^{-1}(\epsilon)$ is generally satisfied. In addition, K_ϵ decreases as ϵ increases, range $K > K_\epsilon$ can be very wide. Hence, in short-range LOS environment, the power allocation map contains one or very few categories outside the OAM beam region.

2) *Very Few Categories in the OAM Beam Regions with High Signal Strength:* From Equation (2), the link gain $g_i^l(r, z)$ can be rewritten as

$$g_i^l(\beta, z) = \frac{\zeta_i^l \lambda_i^2}{(4\pi)^2 (d_{i,m}^l(z))^2} \left(\frac{\lambda_a |l_m|}{\lambda_i |l|} \right)^{|l|} \beta^{2|l|} e^{|l|} e^{-\frac{\lambda_a |l_m|}{\lambda_i} \beta^2}, \quad (24)$$

where λ_a and l_m have been introduced above Equation (14) as an arbitrary carrier wavelength and an arbitrary nonzero OAM mode, respectively. Then, we have that for any z , $g_i^l(\beta, z)$ first increases as β increases within range $0 < \beta < \sqrt{\frac{\lambda_i |l|}{\lambda_a |l_m|}}$, and then decreases as β increases within range $\beta > \sqrt{\frac{\lambda_i |l|}{\lambda_a |l_m|}}$. Specially, for $l = 0$, $g_i^l(\beta, z)$ always decreases as β increases. Denote $\beta_{i,max}^l \triangleq \sqrt{\frac{\lambda_i |l|}{\lambda_a |l_m|}}$ corresponding to the position with the maximum link gain for any z . For any two OAM modes l_1 and l_2 that satisfy $|l_1| > |l_2|$, $a_i^{l_1, l_2}(\beta, z)$ increases as β increases according to Equation (15). However, when both $|l_1|$ and $|l_2|$ are small and $|l_1|$ is close to $|l_2|$, there exist some positions where $a_i^{l_1, l_2}(\beta, z)$ is a moderate value. For instance, for $|l_1| = 1, |l_2| = 0$ and $\zeta_i^{l_1} = \zeta_i^{l_2}$, $a_i^{l_1, l_2}(\beta_{i,max}^{l_1}, z) = e$, which implies that $a_i^{l_1, l_2}(\beta, z)$ is moderate around $\beta_{i,max}^{l_1}$. For short-range LOS links, $g_i^{l_1}(\beta, z)$ is high within this range, and thus $g_i^{l_2}(\beta, z)$

is also high due to moderate $a_i^{l_1, l_2}(\beta, z)$. We consider these regions as the OAM beam regions with high signal strength. In addition, for low noise power, $\frac{N_i}{g_i}$ is very small. Hence, the sum-rate difference ΔR at position 2 using the power allocation of position 0 satisfies Equation (23) for any three positions $q = \{0, 1, 2\}$ with $z_0 = z_1$ and $\beta_1 = \beta_2$. According to Theorem 4, the upper bound denoted as U_o in Equation (18) is small because $P_{sum} \gg \frac{N_i}{g_i}$. This implies that for a given threshold τ_s , although ϵ and U_o at different position 2 are also different, $\epsilon > U_o$ is generally satisfied. Moreover, the features of sum-rate difference within range $0 < K < 1$ are similar to those in the regions outside OAM beam, which implies that K always larger than K_ϵ when link gains in all sub-channels are high. Hence, $\Delta R < \epsilon$ tends to hold, and there will be only one or very few categories.

3) *Multiple Categories in the Boundary Regions of OAM Beams:* In the regions where β is far away from $\beta_{i, max}^l$, $g_i^l(\beta, z)$ in the sub-channel with indexes i and l is low, and thus $\frac{N_i}{g_i}$ is high. We consider these regions as the boundary regions of the OAM beam with mode l in the i -th sub-system. Similarly, considering three positions $q = \{0, 1, 2\}$ with $z_0 = z_1$ and $\beta_1 = \beta_2$, sum-rate difference ΔR at position 2 using the power allocation of position 0 satisfies Equation (23) only when β_2 is sufficiently close to β_0 . In this case, the system can still use a fixed power allocation within a certain range of K . However, when β_2 is not sufficiently close to β_0 , the difference between the optimal power allocation of position 2 and the optimal power allocation of position 0 can be large, which leads to a large sum-rate difference. The property that a large power allocation difference can lead to a large sum-rate difference can be derived from the water-filling algorithm, and the proof is omitted here. In this case, ΔR can be larger than ϵ , and thus position 2 can not be classified into the same category with position 0. Hence, a new category is needed in these regions.

For any $l \neq 0$, assuming $0 < \Delta\beta < \beta_{i, max}^l$, we have

$$a_r \triangleq \frac{g_i^l(\beta_{i, max}^l + \Delta\beta, z)}{g_i^l(\beta_{i, max}^l - \Delta\beta, z)} = \left(1 + \frac{2\Delta\beta}{\beta_{i, max}^l - \Delta\beta}\right)^{2|l|} e^{\frac{|l_m| \lambda_a}{\lambda_i} 4\Delta\beta \beta_{i, max}^l}. \quad (25)$$

Since $\partial a_r / \partial \Delta\beta > 0$ always holds, we have $a_r > a_r|_{\Delta\beta=0} = 1$. This implies that the signal strength in the left boundary regions of OAM beams decays more rapidly than that in right boundary regions as $\Delta\beta$ increases. Hence, ΔR varies greatly in left boundary regions, especially when the noise power in each sub-channel is high. This implies multiple categories in the left boundary regions; and compared with right boundary regions, the areas of these categories are smaller.

E. Simulation Results for Power Allocation Map

Assume short-distance LOS environment and the ranges of z and r are $0.5 \sim 5\text{m}$ and $0.02 \sim 0.3\text{m}$, respectively. Assume that the number of parallel sub-systems is $I = 5$. Assume that all sub-systems have the same bandwidth and thus the same noise power N_0 . We further assume that the parameters of

all sub-systems are the same and $z_R = 2$. The total power $P_{sum} = 1$. The carrier frequency of first sub-system is $60GHz$ and the carrier frequency interval of adjacent sub-systems is Δf .

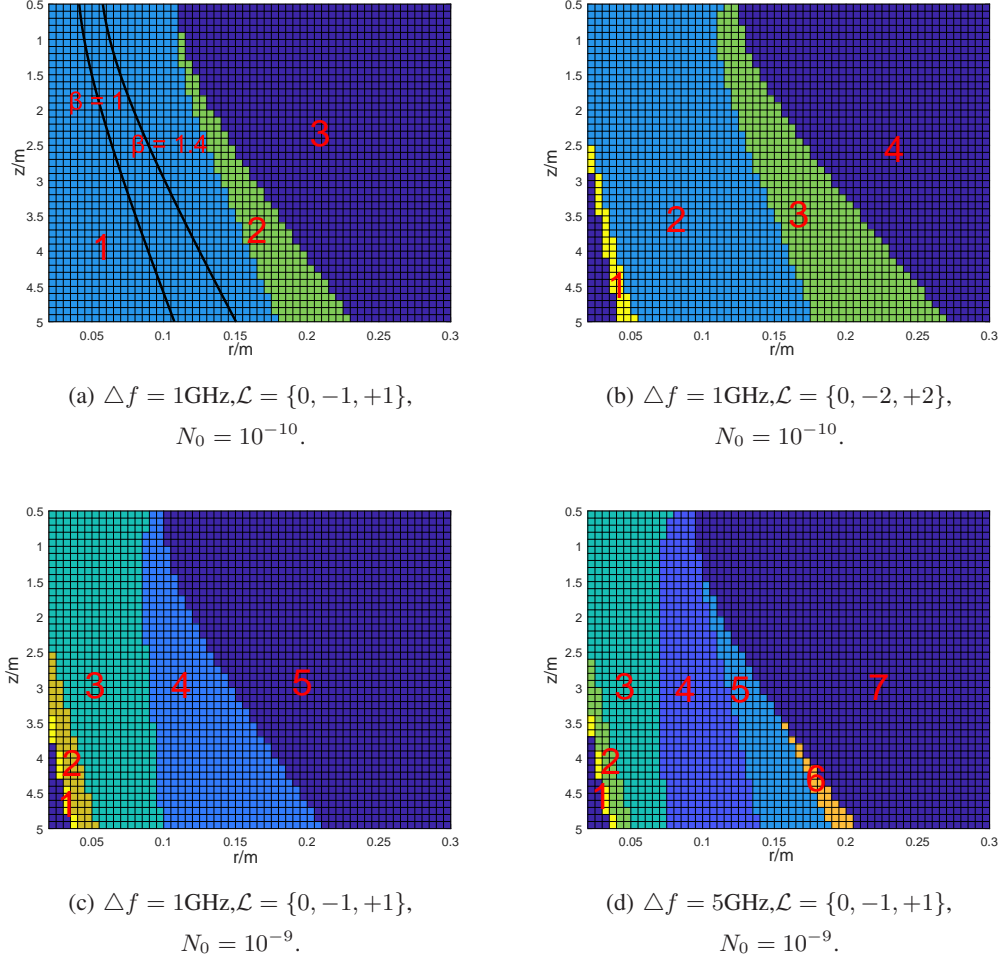


Fig. 7: The power allocation maps with different parameters.

Figure 7 shows the power allocation maps with different system parameters. In Figure 7a, we can observe that the OAM beam regions are only classified into two categories (1 and 2). In category 1, where all OAM beams with different modes can cover, $\frac{N_i}{g_i}$ of each sub-channel i is sufficiently small due to the low noise power ($N_0 = 10^{-10}$), which is consistent with the case introduced in Part III-D2. Hence, fixed power allocation can be adopted in the whole region in category 1. Since the regions in category 2 are the boundary regions of OAM beams with mode 0, the system can not adopt the same power allocation of category 1 according to Part III-D3. Moreover, Figure 7a also gives two curves $\beta r_{a,max}^{l_m}(z)$ with $\beta = 1$ and $\beta = 1.4$, wherein $l_m = +1$ and $\lambda_a = \lambda_1$. It is seen that β determines the horizontal distance from the beam axis, and $r_{a,max}^{l_m}(z)$ determines the direction of the beam diverging as z increases.

Figure 7b considers the OAM beams with modes ± 2 with larger beam divergence than modes ± 1 , where Category 1 represents the left boundary of the OAM beams with modes ± 2 . Since the signal strength in left boundary regions decays rapidly according to Part III-D3, the area of category 1 is small. Categories 2 and 3 are similar to categories 1 and 2 in Figure 7a, respectively. Moreover, from Figures 7a and 7b, we know that the regions of all categories within OAM beam regions diverge approximately along the same set of curves $r_{a,max}^{l_m}(z)$, as z increases.

Figure 7c gives the power allocation map under high noise power ($N_0 = 10^{-9}$). Compared with Figure 7a, there are more categories in left boundary regions of OAM beam with modes ± 1 , which is consistent with the analysis in Part III-D3. Moreover, for the regions near to category 3 in category 4, $\frac{N_i}{g_i}$ of the sub-channels with mode 0 are very large and there is no allocated power for these sub-channels. Thus, the regions in category 3 do not diverge along the same direction in Figure 7a.

When $\Delta f = 5\text{GHz}$, the link gain discrepancy between different sub-systems becomes observable. According to the analysis in Part III-D3, the map in Figure 7d has more categories than that in Figure 7c due to more boundary regions.

In addition, from Figure 7, we can observe that there is only one category in the region outside the OAM beam. This is consistent with the analysis in Part III-D1. Meanwhile, from Figures 7b, 7c and 7d, when r is small and z is large, the signal strength with nonzero OAM mode will be low and the signal strength with OAM mode 0 is dominant. In these regions, the power allocation schemes are similar to those in the region outside the OAM beam and thus classified into one category.

IV. HIGH DIMENSIONAL CONSTELLATION MAP FOR MMWAVE WDM SYSTEMS

In this section, we consider the high dimensional constellation design and analyze the performance loss when adopting map-assisted approach.

A. High Dimensional Constellation Design

We assume that all OAM parallel sub-channels serve one user and can jointly carry one high dimensional symbol. Denote $L = |\mathcal{L}|$ as the number of OAM modes in any sub-system and $U = IL$ as the total number of sub-channels. Since the sub-channels are all orthogonal to each other, we use set $\{1, 2, \dots, U\}$ to represent the sub-channel set. Let $\mathbf{p} \triangleq [P_1, P_2, \dots, P_U]^T$ denote the allocated power vector over all sub-channels. Let $\mathcal{C} \triangleq \{\mathbf{s}_1, \mathbf{s}_2, \dots, \mathbf{s}_M\}$ denote the high dimensional constellation symbol set.

At the receiver, the received signal can be written as

$$\mathbf{y} = \mathbf{Z}\mathbf{H}\mathbf{A}\mathbf{s} + \mathbf{n}, \quad (26)$$

B. MED-difference Analysis on High Dimensional Constellation Map

Since the MED can represent the performance of a high dimensional constellation when the SNRs in each activated sub-channel are high [41], we consider the normalized MED difference as the performance loss of the system at one position using another high dimensional constellation. Because this metric is different with that in power allocation problem, the obtained conclusions of high dimensional constellation map and power allocation map may have some discrepancy.

Generally, different optimization problems may require different maps to store the optimization results due to the different utility functions and parameters. However, for high dimensional constellation design, the optimization problem is constrained by power allocation. Hence, we first consider the influence of power allocation on the normalized MED difference. Assume that \mathbf{p}^* and \mathbf{p}^{map} are the optimal and mapped² power allocation vectors for \mathbf{H} , respectively; \mathcal{C}^* and \mathcal{C}^m are the optimal high dimensional constellations for \mathbf{H} under \mathbf{p}^* and \mathbf{p}^{map} , respectively. Let $d_{min}(\mathbf{H}, \mathbf{p}, \mathcal{C})$ denote the MED under the corresponding conditions. Assume that $\{\mathbf{s}_o^*, \mathbf{s}_o^*\}$ and $\{\mathbf{s}_o^m, \mathbf{s}_o^m\}$ are the corresponding MED constellation pairs for \mathbf{p}^* using \mathcal{C}^* and \mathcal{C}^m , respectively; $\{\mathbf{s}_m^*, \mathbf{s}_m^*\}$ and $\{\mathbf{s}_m^m, \mathbf{s}_m^m\}$ are the corresponding MED constellation pairs for \mathbf{p}^{map} using \mathcal{C}^* and \mathcal{C}^m , respectively. We have the following result on the normalized MED difference.

Theorem 5. *Letting \mathbf{s}_d denote the set of $\{\mathbf{s}_o^* - \mathbf{s}_o^*, \mathbf{s}_o^m - \mathbf{s}_o^m, \mathbf{s}_m^* - \mathbf{s}_m^*, \mathbf{s}_m^m - \mathbf{s}_m^m\}$ and $\mathbf{A}^* = \text{sqr}t(\text{diag}(\mathbf{p}^*))$, we have the following upper bound*

$$d_{loss}^{\mathbf{p}} \triangleq \left| 1 - \frac{d_{min}(\mathbf{H}, \mathbf{p}^{map}, \mathcal{C}^m)}{d_{min}(\mathbf{H}, \mathbf{p}^*, \mathcal{C}^*)} \right| \leq \|\mathbf{p}^* - \mathbf{p}^{map}\|_2 \cdot \max_{\tilde{\mathbf{s}} \in \mathbf{s}_d} \left\{ \frac{\|\mathbf{Z}\mathbf{H}\tilde{\mathbf{s}}\|_2^2}{\|\mathbf{Z}\mathbf{H}\mathbf{A}^*\tilde{\mathbf{s}}\|_2^2} \right\}. \quad (32)$$

Generally, term $\max_{\tilde{\mathbf{s}} \in \mathbf{s}_d} \left\{ \frac{\|\mathbf{Z}\mathbf{H}\tilde{\mathbf{s}}\|_2^2}{\|\mathbf{Z}\mathbf{H}\mathbf{A}^*\tilde{\mathbf{s}}\|_2^2} \right\}$ is finite, we have $d_{loss}^{\mathbf{p}} = O(\|\mathbf{p}^* - \mathbf{p}^{map}\|_2)$.

Proof. See Appendix E. □

Based on Theorem 5, the order of the asymptotic convergence rate of $d_{loss}^{\mathbf{p}}$ with respect to \mathbf{p}^{map} is not larger than the order of $\|\mathbf{p}^* - \mathbf{p}^{map}\|_2$. This indicates that compared with using \mathbf{p}^* to generate high dimensional constellations, the performance loss of using \mathbf{p}^{map} can be sufficiently small if $\|\mathbf{p}^* - \mathbf{p}^{map}\|_2$ is sufficiently small. We consider utilizing \mathbf{p}^{map} to generate the high dimensional constellation since the $\|\mathbf{p}^* - \mathbf{p}^{map}\|_2$ is generally small in each category of the power allocation map.

Then, we consider the influence of channel matrix on the normalized MED difference. Assume that $\mathbf{H}^{(1)}$ and $\mathbf{H}^{(2)}$ are channel matrices at any two positions. If $\mathbf{H}^{(1)}$ and $\mathbf{H}^{(2)}$ satisfy $\mathbf{H}^{(2)} = \alpha\mathbf{H}^{(1)}$, where α is a positive number, the first constraint under $\mathbf{H}^{(2)}$ can be expressed by

$$\mathbf{x}_{\mathbf{p}}^T \mathbf{E}_{ij}^{(2)} \mathbf{x}_{\mathbf{p}} = \alpha^2 \cdot \mathbf{x}_{\mathbf{p}}^T \mathbf{E}_{ij}^{(1)} \mathbf{x}_{\mathbf{p}} \geq d_{min}^2, \quad \forall \tilde{i}, \tilde{j}, 1 \leq \tilde{i} < \tilde{j} \leq M. \quad (33)$$

²The word ‘‘mapped’’ indicates that the system uses the result of the map

It is easy to know that the original optimization problem (30) under $\mathbf{H}^{(2)}$ is equivalent to that under $\mathbf{H}^{(1)}$, with only scaling difference.

For the region outside OAM beam, the variations of the link gains in different sub-channels are proportional according to Equation (5), and thus the system can use a fixed high dimensional constellation in this region. For OAM beam region, these variations are proportional only at the positions with same β , and are not strictly proportional at other positions. Hence, we consider the influence of this non-proportional channel variation. Assume that $\mathbf{H}^{(2)} = \alpha\mathbf{H}^{(1)} + \Delta\mathbf{H}$, where $\Delta\mathbf{H}$ stands for the deviation. Let $\mathcal{C}^{*,(1)}$ and $\mathcal{C}^{*,(2)}$ denote the optimal high dimensional constellations for $\alpha\mathbf{H}^{(1)}$ and $\mathbf{H}^{(2)}$, respectively. Assume that $\{\mathbf{s}_m^{(1)}, \mathbf{s}_{\hat{m}}^{(1)}\}$ and $\{\mathbf{s}_m^{(2)}, \mathbf{s}_{\hat{m}}^{(2)}\}$ are the corresponding MED constellation pairs for $\alpha\mathbf{H}^{(1)}$ using $\mathcal{C}^{*,(1)}$ and $\mathcal{C}^{*,(2)}$, respectively; $\{\mathbf{s}_o^{(1)}, \mathbf{s}_{\hat{o}}^{(1)}\}$ and $\{\mathbf{s}_o^{(2)}, \mathbf{s}_{\hat{o}}^{(2)}\}$ are the corresponding MED constellation pairs for $\mathbf{H}^{(2)}$ using $\mathcal{C}^{*,(1)}$ and $\mathcal{C}^{*,(2)}$, respectively. Then, we have the following result on the normalized MED difference.

Theorem 6. *Given $\mathbf{H}^{(1)}$ and $\mathbf{H}^{(2)}$ that satisfy $\mathbf{H}^{(2)} = \alpha\mathbf{H}^{(1)} + \Delta\mathbf{H}$, we have the following upper bound*

$$d_{loss}^{\Delta\mathbf{H}} \triangleq 1 - \frac{d_{min}(\mathbf{H}^{(2)}, \mathbf{p}, \mathcal{C}^{*,(1)})}{d_{min}(\mathbf{H}^{(2)}, \mathbf{p}, \mathcal{C}^{*,(2)})} \leq \frac{\|\Delta\mathbf{H}\|_F (\|\mathbf{Z}\mathbf{A}(\mathbf{s}_m^{(2)} - \mathbf{s}_{\hat{m}}^{(2)})\|_2 + \|\mathbf{Z}\mathbf{A}(\mathbf{s}_o^{(1)} - \mathbf{s}_{\hat{o}}^{(1)})\|_2)}{\|\mathbf{Z}\mathbf{H}^{(2)}\mathbf{A}(\mathbf{s}_o^{(2)} - \mathbf{s}_{\hat{o}}^{(2)})\|_2}. \quad (34)$$

Generally, term $(\|\mathbf{Z}\mathbf{A}(\mathbf{s}_m^{(2)} - \mathbf{s}_{\hat{m}}^{(2)})\|_2 + \|\mathbf{Z}\mathbf{A}(\mathbf{s}_o^{(1)} - \mathbf{s}_{\hat{o}}^{(1)})\|_2) / \|\mathbf{Z}\mathbf{H}^{(2)}\mathbf{A}(\mathbf{s}_o^{(2)} - \mathbf{s}_{\hat{o}}^{(2)})\|_2$ is finite, we have $d_{loss}^{\Delta\mathbf{H}} = O(\|\Delta\mathbf{H}\|_F)$.

Proof. See Appendix F. □

Since $d_{min}(\mathbf{H}^{(2)}, \mathbf{p}, \mathcal{C}^{*,(2)}) \geq d_{min}(\mathbf{H}^{(2)}, \mathbf{p}, \mathcal{C}^{*,(1)})$ always holds, we have $d_{loss}^{\Delta\mathbf{H}} \geq 0$. Theorem 6 indicates that the order of the asymptotic convergence rate of $d_{loss}^{\Delta\mathbf{H}}$ with respect to $\Delta\mathbf{H}$ is not larger than that of $\|\Delta\mathbf{H}\|_F$. Hence, $d_{loss}^{\Delta\mathbf{H}}$ can be sufficiently small if $\|\Delta\mathbf{H}\|_F$ is sufficiently small, and the systems under $\mathbf{H}^{(1)}$ and $\mathbf{H}^{(2)}$ can use a fixed high dimensional constellation.

As solving high dimensional constellation problem is computationally intensive, we still employ the map to store the high dimensional constellation, and adopt MED d_{min} as the mapping criterion. We utilize the power allocation scheme \mathbf{p}^{map} obtained from power allocation map to generate high dimensional constellation. Let $\mathcal{C}^{m,(q_1)}$ denote the optimal high dimensional constellation of position q_1 under \mathbf{p}^{map} , and $d_{min}(\mathbf{H}^{q_2}, \mathbf{p}^{map}, \mathcal{C}^{m,(q_1)})$ denote the MED of position q_2 using constellation $\mathcal{C}^{m,(q_1)}$. The normalized MED difference for position q_2 using $\mathcal{C}^{m,(q_1)}$ can be expressed as $\Delta\bar{d}_{min}(q_1, q_2) = |1 - d_{min}(\mathbf{H}^{q_2}, \mathbf{p}^{map}, \mathcal{C}^{m,(q_1)}) / d_{min}(\mathbf{H}^{q_2}, \mathbf{p}^{map}, \mathcal{C}^{m,(q_2)})|$. Similarly, we also adopt clustering approach to quantify the constellations of all positions and use one constellation set $\mathcal{C}^{m,(q_1)}$ in each category. Then, the performance loss at other positions q_2 in this category is characterized by $\Delta\bar{d}_{min}(q_1, q_2)$. The clustering algorithm is similar to that in power allocation map. We set $\tau_{d_{min}}$ as the threshold that

determines whether two positions are classified into one category and C_d as the repeat number of the algorithm. In this paper, we set $\tau_{d_{min}} = 0.1$ and $C_d = 100$.

C. Simulation Results for High Dimensional Constellation Map

Assume that $\mathcal{L} = \{-1, 0, +1\}$. The noise powers of all sub-channels are $N_0 = 10^{-10}$ and the number of sub-systems is $I = 2$. The carrier frequencies of the two sub-systems are 60GHz and 65GHz. respectively. We set the number of high dimensional symbols $M = 32$.

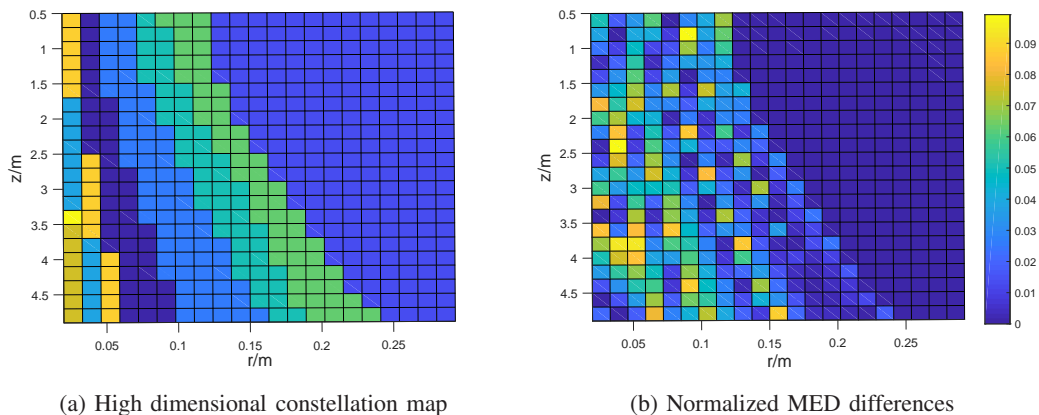


Fig. 8: The high dimensional constellation map and normalized MED differences of the mmWave WDM systems.

Figure 8a gives the high dimensional constellation map. It is observed that the OAM beam regions are classified into multiple categories (8 categories). Compared with power allocation map, high dimensional constellation map is more complicated and needs more categories in OAM beam regions. Meanwhile, it is shown that the region in each category diverge along the same direction as z increases, and in fact, this direction can also be approximated as $r_{a,max}^{l_m}(z)$. According to Theorem 4, the link gain ratio between any two sub-channels remains approximately unchanged for any positions $(\beta r_{a,max}^{l_m}(z), z)$ with fixed β , and thus the channel matrices are close to be proportional. Hence, Figure 8a confirms that the system can employ a fixed constellation if the channel matrices are close to be proportional, which verifies Theorem 6. Moreover, it is seen that the region of the category with small r is smaller than that of the category with large r . The reason is that the link gain of OAM beam in small r regions varies faster than that in large r regions. Figure 8b shows the normalized MED differences $\Delta \bar{d}_{min}(q_1, q_2)$. It is observed that the normalized MED differences are always small in the region outside the OAM beam. The reason is that the link gain ratios in these regions are uniform, which indicates that $\Delta \mathbf{H} = 0$, and

thus the generated high dimensional constellations are the same. We observe that the normalized MED differences are irregular in the OAM beam region. The reason is that the normalized MED differences are not uniform continuous with respect to $\|\Delta\mathbf{H}\|_F$, which means that the normalized MED differences are not exactly the same even if the $\Delta\mathbf{H}$ are the same at different positions. Furthermore, the solution of the approximated optimization problem using iterative algorithm may be not global optimal. Hence, the normalized MED difference may fluctuate within the OAM beam region.

In summary, for short-range LOS links, high dimensional constellation map is complicated in the OAM beam regions and we need to classify these regions into more categories than the power allocation map. However, it is worth mentioning that as the number of OAM modes and wavelengths increases, the high dimensional constellation map will become more complicated. High dimensional constellation map can be adopted when the number of sub-channels is small.

V. CONCLUSION

In this paper, we consider a mmWave WDM system with positioning information in short-range LOS environment. We also consider the OAM multiplexing in each wavelength part. Based on the quasi-static feature of the communication links, we have proposed a map-assisted approach to offline store the system parameters according to the transceiver's position and configure the system by employing these parameters when obtaining the position information. To reduce the storage and search complexity, we attempt to classify all considered positions into several categories and employ one fixed parameter in each category. We have applied the map-assisted method to two problems: power allocation and high dimensional constellation design. For power allocation problem, we have discussed the sum-rate difference of employing the fixed power allocation. It can be observed that the sum-rate difference is small within plane wave only region and the system can employ a fixed power allocation. Whereas for OAM beam region, the features of sum-rate difference are similar to that in plane wave region only at certain positions. We have also analyzed the characteristics of high dimensional constellation, and figured out that the normalized MED difference of fixed constellation is sufficiently small if channel matrices are sufficiently close to be proportional under fixed power allocation. Numerical analyses have also been performed to verify the theoretical analysis.

VI. ACKNOWLEDGMENTS

The authors would like to thank Dr. Qian Gao (Futurewei Technology) for his constructive comments and suggestions that improve the quality of this paper.

APPENDIX A
PROOF OF THEOREM 1

Combining Equation (8), we have

$$-\log_2 \left[1 + \frac{\frac{\lambda_1^2 N_1}{g_1^{(1)}} (K-1) \left(\sum_{j=1}^I \frac{\xi_j}{\lambda_j^2} - \frac{I \xi_i}{\lambda_i^2} \right)}{K P_{sum} + \frac{\lambda_1^2 N_1}{g_1^{(1)}} \sum_{j=1}^I \frac{\xi_j}{\lambda_j^2}} \right] = -\log_2 \left[\frac{I \left(\frac{N_i}{g_i^{(1)}} + K P_i^{*(1)} \right)}{K P_{sum} + \frac{\lambda_1^2 N_1}{g_1^{(1)}} \sum_{j=1}^I \frac{\xi_j}{\lambda_j^2}} \right]. \quad (35)$$

Letting $a = \frac{\lambda_1^2 N_1}{g_1^{(1)}}$ and $b = \sum_{j=1}^I \frac{\xi_j}{\lambda_j^2}$, we have $\Delta R_i = -\log_2 \left[1 + \frac{a(K-1)(b - \frac{I \xi_i}{\lambda_i^2})}{K P_{sum} + ab} \right]$. From Equation (35),

it is observed that term $1 + \frac{a(K-1)(b - \frac{I \xi_i}{\lambda_i^2})}{K P_{sum} + ab} > 0$ due to $P_i^{*(1)} \geq 0$. Then, we have

$$\frac{\partial R_i}{\partial K} = \frac{-\log_2 e \cdot a \left(b - \frac{I \xi_i}{\lambda_i^2} \right) (P_{sum} + ab)}{(K P_{sum} + ab)^2 \left[1 + \frac{a(K-1)(b - \frac{I \xi_i}{\lambda_i^2})}{K P_{sum} + ab} \right]}. \quad (36)$$

For the i -th sub-channel, if $(b - \frac{I \xi_i}{\lambda_i^2}) < 0$, we have

$$\frac{\partial \Delta R_i}{\partial K} > \frac{-\log_2 e \cdot a \left(b - \frac{I \xi_i}{\lambda_i^2} \right) (P_{sum} + ab)}{(K P_{sum} + ab)^2} > 0. \quad (37)$$

If $(b - \frac{I \xi_i}{\lambda_i^2}) > 0$, we have

$$0 > \frac{\partial \Delta R_i}{\partial K} > \frac{-\log_2 e \cdot a \left(b - \frac{I \xi_i}{\lambda_i^2} \right) (P_{sum} + ab)}{(K P_{sum} + ab)^2}. \quad (38)$$

Hence, we have

$$\frac{\partial \Delta R}{\partial K} = \sum_{i=1}^I \frac{\partial \Delta R_i}{\partial K} > \sum_{i=1}^I \frac{-\log_2 e \cdot a \left(b - \frac{I \xi_i}{\lambda_i^2} \right) (P_{sum} + ab)}{(K P_{sum} + ab)^2} = 0. \quad (39)$$

It is seen that sum-rate difference increases with K for $K > 1$ and

$$\lim_{K \rightarrow \infty} \Delta R = -\log_2 \prod_{i=1}^I \left[1 + \frac{\frac{\lambda_1^2 N_1}{g_1^{(1)}} \left(\sum_{j=1}^I \frac{\xi_j}{\lambda_j^2} - \frac{I \xi_i}{\lambda_i^2} \right)}{P_{sum}} \right], \quad (40)$$

which is an upper bound independent of K .

Then, letting $A_i = \log_2 e \cdot a \left(b - \frac{I \xi_i}{\lambda_i^2} \right) (P_{sum} + ab)$, the second-order partial derivative of rate difference with respect to K can be written as

$$\frac{\partial^2 \Delta R_i}{\partial K^2} = \frac{A_i \cdot P_{sum}}{(K P_{sum} + ab)^3 \left[1 + \frac{a(K-1)(b - \frac{I \xi_i}{\lambda_i^2})}{K P_{sum} + ab} \right]} + \frac{A_i \left[P_{sum} + a \left(b - \frac{I \xi_i}{\lambda_i^2} \right) \right]}{(K P_{sum} + ab)^3 \left[1 + \frac{a(K-1)(b - \frac{I \xi_i}{\lambda_i^2})}{K P_{sum} + ab} \right]^2}. \quad (41)$$

When K approaches 1, we have

$$\frac{A_i \left[P_{sum} + a \left(b - \frac{I \xi_i}{\lambda_i^2} \right) \right]}{(K P_{sum} + ab)^3 \left[1 + \frac{a(K-1)(b - \frac{I \xi_i}{\lambda_i^2})}{K P_{sum} + ab} \right]^2} > \frac{A_i \cdot P_{sum}}{(K P_{sum} + ab)^3}. \quad (42)$$

For the i -th sub-channel, if the following formula is satisfied

$$\begin{aligned} & \frac{A_i \left[P_{sum} + a \left(b - \frac{I\xi_i}{\lambda_i^2} \right) \right]}{(K P_{sum} + ab)^3 \left[1 + \frac{a(K-1)(b - \frac{I\xi_i}{\lambda_i^2})}{K P_{sum} + ab} \right]^2} - \frac{A_i \cdot P_{sum}}{(K P_{sum} + ab)^3} \\ & > \frac{A_i \cdot P_{sum}}{(K P_{sum} + ab)^3} - \frac{A_i \cdot P_{sum}}{(K P_{sum} + ab)^3 \left[1 + \frac{a(K-1)(b - \frac{I\xi_i}{\lambda_i^2})}{K P_{sum} + ab} \right]}, \end{aligned} \quad (43)$$

we have $\frac{\partial^2 \Delta R_i}{\partial K^2} > \frac{2A_i \cdot P_{sum}}{(K P_{sum} + ab)^3}$. Since $1 + \frac{a(K-1)(b - \frac{I\xi_i}{\lambda_i^2})}{K P_{sum} + ab} \approx 1$ when K approaches to 1, Equations (42) and (43) are satisfied simultaneously, leading to $\frac{\partial^2 \Delta R}{\partial K^2} = \sum_{i=1}^I \frac{\partial^2 \Delta R_i}{\partial K^2} > \sum_{i=1}^I \frac{2A_i \cdot P_{sum}}{(K P_{sum} + ab)^3} = 0$. As K increases, $\left| \frac{a(K-1)(b - \frac{I\xi_i}{\lambda_i^2})}{K P_{sum} + ab} \right|$ also increases and Equation (43) will not hold for some sub-channels, leading to $\frac{\partial^2 \Delta R}{\partial K^2} = \sum_{i=1}^I \frac{\partial^2 \Delta R_i}{\partial K^2} < 0$. As K further increases, Equations (42) and (43) are not satisfied, but $\frac{\partial^2 \Delta R}{\partial K^2} < 0$ still holds. Hence, letting K_0 satisfies $\frac{\partial^2 \Delta R}{\partial K^2} |_{K=K_0} = 0$, $\frac{\partial^2 \Delta R}{\partial K^2} < 0$ always holds within the range of $K > K_0$.

However, it is difficult to obtain the closed form of K_0 . Then, we give an upper bound on K_0 . From the above analysis, $\frac{\partial^2 \Delta R}{\partial K^2} < 0$ when Equation (43) doesn't hold for all sub-channels. Hence, we have

$$\begin{aligned} & A_i \left[P_{sum} + a \left(b - \frac{I\xi_i}{\lambda_i^2} \right) \right] - 2A_i P_{sum} \left[1 + \frac{a(K-1)(b - \frac{I\xi_i}{\lambda_i^2})}{K P_{sum} + ab} \right]^2 \\ & + A_i P_{sum} \left[1 + \frac{a(K-1)(b - \frac{I\xi_i}{\lambda_i^2})}{K P_{sum} + ab} \right] < 0. \end{aligned} \quad (44)$$

For the i -th sub-channel, it is easy to get the solution of Equation (44) as

$$K > \frac{a \left[\frac{1}{4}b + \sqrt{\frac{9}{16} + \frac{a}{2P_{sum}}(b - \frac{I\xi_i}{\lambda_i^2})} b - \frac{I\xi_i}{\lambda_i^2} \right]}{a(b - \frac{I\xi_i}{\lambda_i^2}) + \left[\frac{3}{4} - \sqrt{\frac{9}{16} + \frac{a}{2P_{sum}}(b - \frac{I\xi_i}{\lambda_i^2})} \right] P_{sum}}. \quad (45)$$

We take the intersection of the solutions of all sub-channels and the upper bound of K_0 can be calculated by

$$K_{0,ub} = \max_i \left\{ \frac{\frac{\lambda_1^2 N_1}{g_1^{(1)}} \left[\frac{1}{4} \sum_{j=1}^I \frac{\xi_j}{\lambda_j^2} + \sqrt{\frac{9}{16} + \frac{\lambda_1^2 N_1}{2g_1^{(1)} P_{sum}} \left(\sum_{j=1}^I \frac{\xi_j}{\lambda_j^2} - \frac{I\xi_i}{\lambda_i^2} \right) \sum_{j=1}^I \frac{\xi_j}{\lambda_j^2} - \frac{I\xi_i}{\lambda_i^2} \right]}{\frac{\lambda_1^2 N_1}{g_1^{(1)}} \left(\sum_{j=1}^I \frac{\xi_j}{\lambda_j^2} - \frac{I\xi_i}{\lambda_i^2} \right) + \left[\frac{3}{4} - \sqrt{\frac{9}{16} + \frac{\lambda_1^2 N_1}{2g_1^{(1)} P_{sum}} \left(\sum_{j=1}^I \frac{\xi_j}{\lambda_j^2} - \frac{I\xi_i}{\lambda_i^2} \right) \right] P_{sum}} \right\}. \quad (46)$$

It is worth mentioning that $\frac{\lambda_1^2 N_1}{2g_1^{(1)} P_{sum}} \left(\sum_{j=1}^I \frac{\xi_j}{\lambda_j^2} - \frac{I\xi_i}{\lambda_i^2} \right)$ approaches to 0 as the SNR increases. Hence, $K_{0,ub}$ is close to 1 in high SNR environment.

APPENDIX B

PROOF OF THEOREM 2

According to Equation (8), we know that $\Delta \dot{R}$ is derived from $P_i^{*(1)}$ and $P_i^{*(2)}$, $1 \leq i \leq I$. However, within range $0 < K < K_{min}$, $P_i^{*(2)}$ is negative if we still use equation $P_i^{*(2)} =$

$\frac{P_{sum}}{I} + \frac{\lambda_1^2 N_1}{K g_1^{(1)}} \left(\frac{1}{I} \sum_{j=1}^I \frac{\xi_j}{\lambda_j^2} - \frac{\xi_i}{\lambda_i^2} \right)$. Hence, $\Delta \dot{R}$ is the ‘‘ideal’’ sum-rate difference without non-negative power constraint; and if the non-negative power constraint in Equation (3) holds, the allocated powers in some sub-channels are 0, which causes that $\Delta R \neq \Delta \dot{R}$. Moreover, since $\Delta \dot{R}$ is the ‘‘ideal’’ value of ΔR , it is easy to have that $\Delta R \leq \Delta \dot{R}$ within range $0 < K < K_{min}$.

When $0 < K < 1$, $K - 1 < 0$ always holds. According to Equation (36), if $(b - \frac{I\xi_i}{\lambda_i^2}) < 0$ is satisfied for the i -th sub-channel, we have

$$\frac{-\log_2 e \cdot a(b - \frac{I\xi_i}{\lambda_i^2})(P_{sum} + ab)}{(KP_{sum} + ab)^2} > \frac{\partial \Delta \dot{R}_i}{\partial K} > 0. \quad (47)$$

If $(b - \frac{I\xi_i}{\lambda_i^2}) > 0$, we have

$$0 > \frac{-\log_2 e \cdot a(b - \frac{I\xi_i}{\lambda_i^2})(P_{sum} + ab)}{(KP_{sum} + ab)^2} > \frac{\partial \Delta \dot{R}_i}{\partial K}. \quad (48)$$

Then, we have

$$\frac{\partial \Delta \dot{R}}{\partial K} = \sum_{i=1}^I \frac{\partial \Delta \dot{R}_i}{\partial K} < 0. \quad (49)$$

Hence, it is known that $\Delta \dot{R}$ decreases monotonically with K within range $0 < K < 1$ and we have

$$\Delta R \leq \Delta \dot{R} \leq \Delta \dot{R}|_{K=0} = \log_2 \prod_{i=1}^I \left(\frac{\lambda_i^2}{\xi_i} \right) + I \log_2 \left(\frac{1}{I} \sum_{j=1}^I \frac{\xi_j}{\lambda_j^2} \right). \quad (50)$$

For the range $K_{min} < K < 1$, $\Delta R = \Delta \dot{R}$ and we have $\frac{\partial \Delta R}{\partial K} = \sum_{i=1}^I \frac{\partial \Delta R_i}{\partial K} < 0$. Meanwhile, $P_{sum} + a(b - \frac{I\xi_i}{\lambda_i^2}) > 0$ always satisfies within this range. According to Equation (41), if $(b - \frac{I\xi_i}{\lambda_i^2}) < 0$ is satisfied for the i -th sub-channel, we have

$$0 > \frac{\partial^2 \Delta R_i}{\partial K^2} > \frac{A_i \left[2P_{sum} + a(b - \frac{I\xi_i}{\lambda_i^2}) \right]}{(KP_{sum} + ab)^3} > \frac{2A_i \cdot P_{sum}}{(KP_{sum} + ab)^3}. \quad (51)$$

If $(b - \frac{I\xi_i}{\lambda_i^2}) > 0$ is satisfied, we have

$$\frac{\partial^2 \Delta R_i}{\partial K^2} > \frac{A_i \left[2P_{sum} + a(b - \frac{I\xi_i}{\lambda_i^2}) \right]}{(KP_{sum} + ab)^3} > \frac{2A_i \cdot P_{sum}}{(KP_{sum} + ab)^3} > 0. \quad (52)$$

Hence we have

$$\frac{\partial^2 \Delta R}{\partial K^2} = \sum_{i=1}^I \frac{\partial^2 \Delta R_i}{\partial K^2} > \sum_{i=1}^I \frac{2A_i \cdot P_{sum}}{(KP_{sum} + ab)^3} = 0. \quad (53)$$

Similarly, we have $\frac{\partial^3 \Delta R}{\partial K^3} < 0$ using the same method. Thus, within range $K_{min} < K < 1$, $\frac{\partial \Delta R}{\partial K} < 0$, $\frac{\partial^2 \Delta R}{\partial K^2} > 0$ and $\frac{\partial^3 \Delta R}{\partial K^3} < 0$ always hold.

APPENDIX C
PROOF OF LEMMA 1

Let $f(x) = \log(1+x)$. Since $f(x)$ is concave in the domain $x > -1$, the inequality $f(y) \leq f(x) + f'(x)(y-x)$ always holds. If a_i and b_i satisfy $a_i b_i \geq 0$ and $a_i + b_i > -1$, we have

$$\log(1+a_i+b_i) \leq \log(1+a_i) + \frac{b_i}{1+a_i}, \quad (54)$$

where $1 \leq i \leq n$. The set $\{i|a_i b_i \geq 0\}$ can be divided into three mutually exclusive sets $\{i|a_i < 0, b_i \leq 0\}$, $\{i|a_i > 0, b_i \geq 0\}$ and $\{i|a_i = 0\}$. For any $a_i < 0$ and $b_i \leq 0$, we can get $a_i > -1$ according to $a_i + b_i > -1$. Thus, $\frac{1}{1+a_i} > 1$ always holds, and we further have $\frac{b_i}{1+a_i} \leq b_i$. For any $a_i > 0$ and $b_i \geq 0$, we can get $0 < \frac{1}{1+a_i} < 1$, and then, we have $\frac{b_i}{1+a_i} \leq b_i$. For any $a_i = 0$, we can easily get $\frac{b_i}{1+a_i} = b_i$. Hence, the above results can lead to the following inequality

$$\log(1+a_i+b_i) \leq \log(1+a_i) + \frac{b_i}{1+a_i} \leq \log(1+a_i) + b_i. \quad (55)$$

If $\sum_{i=1}^n b_i = 0$, we have

$$\sum_{i=1}^n \log(1+a_i+b_i) \leq \sum_{i=1}^n \log(1+a_i) + \sum_{i=1}^n b_i = \sum_{i=1}^n \log(1+a_i), \quad (56)$$

which can readily lead to the inequality $\prod_{i=1}^n (1+a_i+b_i) \leq \prod_{i=1}^n (1+a_i)$.

APPENDIX D
PROOF OF THEOREM 3

Denote

$$\varrho_i \triangleq \frac{\frac{\lambda_1^2 N_1}{g_1^{(1)}} (K-1) (\sum_{j=1}^I \frac{\xi_j}{\lambda_j^2} - \frac{I \xi_i}{\lambda_i^2})}{K P_{sum} + \frac{\lambda_1^2 N_1}{g_1^{(1)}} \cdot \sum_{j=1}^I \frac{\xi_j}{\lambda_j^2}}, \quad \nu_i \triangleq \frac{\frac{\lambda_1^2 N_1}{g_1^{(1)}} (\sum_{j=1}^I \frac{\xi_j}{\lambda_j^2} - \frac{I \xi_i}{\lambda_i^2})}{P_{sum}}. \quad (57)$$

Since $|\varrho_i|$ for $1 \leq i \leq I$ decreases as $\frac{g_1^{(1)}}{N_1}$ increases, $\prod_{i=1}^I (1+\varrho_i)$ increases based on Lemma 1. According to Equation (12), upper bound $\Delta \hat{R}$ of sum-rate difference for any $0 < K < 1$ also decreases as $\frac{g_1^{(1)}}{N_1}$ increases. Assume that $\Delta \hat{R}_1$ and $\Delta \hat{R}_2$ are the corresponding upper bounds in Equation (12) under two channel conditions $\frac{g_1^{(1)}}{N_1} = \varpi_1$ and $\frac{g_1^{(1)}}{N_1} = \varpi_2$, respectively, where $(\frac{g_1^{(1)}}{N_1})_{min} < \varpi_1 < \varpi_2$. For any $K_{\epsilon_1,1}$ satisfying $0 < K_{\epsilon_1,1} < 1$, assuming that $K_{\epsilon_1,1} = \Delta \hat{R}_1^{-1}(\epsilon_1) = \Delta \hat{R}_2^{-1}(\epsilon_2)$, we have $\epsilon_1 > \epsilon_2$. Since $\Delta \hat{R}_2$ decreases monotonically with K within range $0 < K < 1$, we have $K_{\epsilon_1,2} = \Delta \hat{R}_2^{-1}(\epsilon_1) < \Delta \hat{R}_2^{-1}(\epsilon_2) = K_{\epsilon_1,1}$, which indicates that K_ϵ decreases as $\frac{g_1^{(1)}}{N_1}$ increases. Moreover, within range $K_\epsilon < K < 1$, $\Delta \hat{R} < \epsilon$ always holds, and such range expands as $\frac{g_1^{(1)}}{N_1}$ increases. However, from Equation (12), it is observed that $\Delta \hat{R}^u$ is independent of $\frac{g_1^{(1)}}{N_1}$. Then, since $|\nu_i|$ for $1 \leq i \leq I$ decreases as $\frac{g_1^{(1)}}{N_1}$ increases, $\prod_{i=1}^I (1+\nu_i)$ increases based on Lemma 1, and thus the upper bound of sum-rate difference in Equation (10) also decreases.

APPENDIX E

PROOF OF THEOREM 5

Letting $\mathbf{A}^* = \text{sqrt}(\text{diag}(\mathbf{p}^*))$ and $\mathbf{A}^{map} = \text{sqrt}(\text{diag}(\mathbf{p}^{map}))$, we first consider the following normalized MED difference,

$$\begin{aligned} & \left| 1 - \frac{d_{\min}(\mathbf{H}, \mathbf{p}^{map}, \mathcal{C}^m)}{d_{\min}(\mathbf{H}, \mathbf{p}^*, \mathcal{C}^m)} \right| \leq \left| 1 - \frac{d_{\min}^2(\mathbf{H}, \mathbf{p}^{map}, \mathcal{C}^m)}{d_{\min}^2(\mathbf{H}, \mathbf{p}^*, \mathcal{C}^m)} \right| = \left| 1 - \frac{\|\mathbf{ZHA}^{map}(\mathbf{s}_m^m - \mathbf{s}_{\hat{m}}^m)\|_2^2}{\|\mathbf{ZHA}^*(\mathbf{s}_o^m - \mathbf{s}_{\hat{o}}^m)\|_2^2} \right| \\ & \leq \max \left\{ \left| 1 - \frac{\|\mathbf{ZHA}^{map}(\mathbf{s}_m^m - \mathbf{s}_{\hat{m}}^m)\|_2^2}{\|\mathbf{ZHA}^*(\mathbf{s}_m^m - \mathbf{s}_{\hat{m}}^m)\|_2^2} \right|, \left| 1 - \frac{\|\mathbf{ZHA}^{map}(\mathbf{s}_o^m - \mathbf{s}_{\hat{o}}^m)\|_2^2}{\|\mathbf{ZHA}^*(\mathbf{s}_o^m - \mathbf{s}_{\hat{o}}^m)\|_2^2} \right| \right\}, \end{aligned} \quad (58)$$

where

$$\begin{aligned} & \left| 1 - \frac{\|\mathbf{ZHA}^{map}(\mathbf{s}_m^m - \mathbf{s}_{\hat{m}}^m)\|_2^2}{\|\mathbf{ZHA}^*(\mathbf{s}_m^m - \mathbf{s}_{\hat{m}}^m)\|_2^2} \right| = \frac{\left| \sum_{i=1}^N \frac{|h_i|^2}{N_i} (p_i^* - p_i^{map}) |\mathbf{s}_m^m(i) - \mathbf{s}_{\hat{m}}^m(i)|^2 \right|}{\|\mathbf{ZHA}^*(\mathbf{s}_m^m - \mathbf{s}_{\hat{m}}^m)\|_2^2} \\ & \leq \frac{\sum_{i=1}^N \frac{|h_i|^2}{N_i} |p_i^* - p_i^{map}| \cdot |\mathbf{s}_m^m(i) - \mathbf{s}_{\hat{m}}^m(i)|^2}{\|\mathbf{ZHA}^*(\mathbf{s}_m^m - \mathbf{s}_{\hat{m}}^m)\|_2^2} \\ & \leq \frac{\left(\sum_{i=1}^N \frac{|h_i|^4}{N_i^2} |\mathbf{s}_m^m(i) - \mathbf{s}_{\hat{m}}^m(i)|^4 \right)^{\frac{1}{2}} \cdot \left(\sum_{i=1}^N |p_i^* - p_i^{map}|^2 \right)^{\frac{1}{2}}}{\|\mathbf{ZHA}^*(\mathbf{s}_m^m - \mathbf{s}_{\hat{m}}^m)\|_2^2} \\ & \leq \frac{\left(\sum_{i=1}^N \frac{|h_i|^2}{N_i} |\mathbf{s}_m^m(i) - \mathbf{s}_{\hat{m}}^m(i)|^2 \right) \cdot \|\mathbf{p}^* - \mathbf{p}^{map}\|_2}{\|\mathbf{ZHA}^*(\mathbf{s}_m^m - \mathbf{s}_{\hat{m}}^m)\|_2^2} \\ & = \frac{\|\mathbf{ZH}(\mathbf{s}_m^m - \mathbf{s}_{\hat{m}}^m)\|_2^2 \cdot \|\mathbf{p}^* - \mathbf{p}^{map}\|_2}{\|\mathbf{ZHA}^*(\mathbf{s}_m^m - \mathbf{s}_{\hat{m}}^m)\|_2^2}. \end{aligned} \quad (59)$$

Similarly, we can obtain the upper bound of $|1 - \|\mathbf{ZHA}^{map}(\mathbf{s}_o^m - \mathbf{s}_{\hat{o}}^m)\|_2^2 / \|\mathbf{ZHA}^*(\mathbf{s}_o^m - \mathbf{s}_{\hat{o}}^m)\|_2^2|$. Hence, the upper bound of $|1 - d_{\min}(\mathbf{H}, \mathbf{p}^{map}, \mathcal{C}^m) / d_{\min}(\mathbf{H}, \mathbf{p}^*, \mathcal{C}^m)|$ can be written as

$$\left| 1 - \frac{d_{\min}(\mathbf{H}, \mathbf{p}^{map}, \mathcal{C}^m)}{d_{\min}(\mathbf{H}, \mathbf{p}^*, \mathcal{C}^m)} \right| \leq \|\mathbf{p}^* - \mathbf{p}^{map}\|_2 \cdot \max \left\{ \frac{\|\mathbf{ZH}(\mathbf{s}_m^m - \mathbf{s}_{\hat{m}}^m)\|_2^2}{\|\mathbf{ZHA}^*(\mathbf{s}_m^m - \mathbf{s}_{\hat{m}}^m)\|_2^2}, \frac{\|\mathbf{ZH}(\mathbf{s}_o^m - \mathbf{s}_{\hat{o}}^m)\|_2^2}{\|\mathbf{ZHA}^*(\mathbf{s}_o^m - \mathbf{s}_{\hat{o}}^m)\|_2^2} \right\}. \quad (60)$$

Since the normalized MED difference $|1 - d_{\min}(\mathbf{H}, \mathbf{p}^{map}, \mathcal{C}^m) / d_{\min}(\mathbf{H}, \mathbf{p}^*, \mathcal{C}^*)|$ satisfies

$$\left| 1 - \frac{d_{\min}(\mathbf{H}, \mathbf{p}^{map}, \mathcal{C}^m)}{d_{\min}(\mathbf{H}, \mathbf{p}^*, \mathcal{C}^*)} \right| \leq \max \left\{ \left| 1 - \frac{d_{\min}(\mathbf{H}, \mathbf{p}^{map}, \mathcal{C}^m)}{d_{\min}(\mathbf{H}, \mathbf{p}^*, \mathcal{C}^m)} \right|, \left| 1 - \frac{d_{\min}(\mathbf{H}, \mathbf{p}^{map}, \mathcal{C}^*)}{d_{\min}(\mathbf{H}, \mathbf{p}^*, \mathcal{C}^*)} \right| \right\}, \quad (61)$$

we have

$$\left| 1 - \frac{d_{\min}(\mathbf{H}, \mathbf{p}^{map}, \mathcal{C}^m)}{d_{\min}(\mathbf{H}, \mathbf{p}^*, \mathcal{C}^*)} \right| \leq \|\mathbf{p}^* - \mathbf{p}^{map}\|_2 \cdot \max_{\tilde{\mathbf{s}} \in \mathbf{s}_d} \left\{ \frac{\|\mathbf{ZH}\tilde{\mathbf{s}}\|_2^2}{\|\mathbf{ZHA}^*\tilde{\mathbf{s}}\|_2^2} \right\}, \quad (62)$$

where \mathbf{s}_d is the set of $\{\mathbf{s}_o^* - \mathbf{s}_{\hat{o}}^*, \mathbf{s}_o^m - \mathbf{s}_{\hat{o}}^m, \mathbf{s}_m^* - \mathbf{s}_{\hat{m}}^*, \mathbf{s}_m^m - \mathbf{s}_{\hat{m}}^m\}$. Given a proper τ_s , the system generally activates the same sub-channels when using \mathbf{p}^{map} or \mathbf{p}^* . Hence, the term $\|\mathbf{ZHA}^*\tilde{\mathbf{s}}\|_2^2$ is non-zero and the term $\max_{\tilde{\mathbf{s}} \in \mathbf{s}_d} \left\{ \frac{\|\mathbf{ZH}\tilde{\mathbf{s}}\|_2^2}{\|\mathbf{ZHA}^*\tilde{\mathbf{s}}\|_2^2} \right\}$ is finite.

APPENDIX F
PROOF OF THEOREM 6

let $\mathbf{A} = \text{sqrt}(\text{diag}(\mathbf{p}))$. According to the definition of MED, we have

$$\begin{aligned}
& 1 - \frac{d_{\min}(\mathbf{H}^{(2)}, \mathbf{p}, \mathcal{C}^{*,(1)})}{d_{\min}(\mathbf{H}^{(2)}, \mathbf{p}, \mathcal{C}^{*,(2)})} = 1 - \frac{\|\mathbf{Z}(\alpha\mathbf{H}^{(1)} + \Delta\mathbf{H})\mathbf{A}(\mathbf{s}_o^{(1)} - \mathbf{s}_\delta^{(1)})\|_2}{\|\mathbf{ZH}^{(2)}\mathbf{A}(\mathbf{s}_o^{(2)} - \mathbf{s}_\delta^{(2)})\|_2} \\
& \leq 1 - \frac{\|\mathbf{Z}\alpha\mathbf{H}^{(1)}\mathbf{A}(\mathbf{s}_o^{(1)} - \mathbf{s}_\delta^{(1)})\|_2 - \|\mathbf{Z}\Delta\mathbf{H}\mathbf{A}(\mathbf{s}_o^{(1)} - \mathbf{s}_\delta^{(1)})\|_2}{\|\mathbf{ZH}^{(2)}\mathbf{A}(\mathbf{s}_o^{(2)} - \mathbf{s}_\delta^{(2)})\|_2} \\
& \leq 1 - \frac{\|\mathbf{Z}\alpha\mathbf{H}^{(1)}\mathbf{A}(\mathbf{s}_m^{(1)} - \mathbf{s}_{\hat{m}}^{(1)})\|_2 - \|\mathbf{Z}\Delta\mathbf{H}\mathbf{A}(\mathbf{s}_o^{(1)} - \mathbf{s}_\delta^{(1)})\|_2}{\|\mathbf{ZH}^{(2)}\mathbf{A}(\mathbf{s}_o^{(2)} - \mathbf{s}_\delta^{(2)})\|_2} \\
& \leq 1 - \frac{\|\mathbf{Z}\alpha\mathbf{H}^{(1)}\mathbf{A}(\mathbf{s}_m^{(2)} - \mathbf{s}_{\hat{m}}^{(2)})\|_2 - \|\mathbf{Z}\Delta\mathbf{H}\mathbf{A}(\mathbf{s}_o^{(1)} - \mathbf{s}_\delta^{(1)})\|_2}{\|\mathbf{ZH}^{(2)}\mathbf{A}(\mathbf{s}_o^{(2)} - \mathbf{s}_\delta^{(2)})\|_2} \\
& \leq 1 - \frac{\|\mathbf{ZH}^{(2)}\mathbf{A}(\mathbf{s}_m^{(2)} - \mathbf{s}_{\hat{m}}^{(2)})\|_2 - \|\mathbf{Z}\Delta\mathbf{H}\mathbf{A}(\mathbf{s}_m^{(2)} - \mathbf{s}_{\hat{m}}^{(2)})\|_2 - \|\mathbf{Z}\Delta\mathbf{H}\mathbf{A}(\mathbf{s}_o^{(1)} - \mathbf{s}_\delta^{(1)})\|_2}{\|\mathbf{ZH}^{(2)}\mathbf{A}(\mathbf{s}_o^{(2)} - \mathbf{s}_\delta^{(2)})\|_2} \\
& \leq 1 - \frac{\|\mathbf{ZH}^{(2)}\mathbf{A}(\mathbf{s}_o^{(2)} - \mathbf{s}_\delta^{(2)})\|_2 - \|\mathbf{Z}\Delta\mathbf{H}\mathbf{A}(\mathbf{s}_m^{(2)} - \mathbf{s}_{\hat{m}}^{(2)})\|_2 - \|\mathbf{Z}\Delta\mathbf{H}\mathbf{A}(\mathbf{s}_o^{(1)} - \mathbf{s}_\delta^{(1)})\|_2}{\|\mathbf{ZH}^{(2)}\mathbf{A}(\mathbf{s}_o^{(2)} - \mathbf{s}_\delta^{(2)})\|_2} \\
& \leq \frac{\|\mathbf{Z}\Delta\mathbf{H}\mathbf{A}(\mathbf{s}_m^{(2)} - \mathbf{s}_{\hat{m}}^{(2)})\|_2 + \|\mathbf{Z}\Delta\mathbf{H}\mathbf{A}(\mathbf{s}_o^{(1)} - \mathbf{s}_\delta^{(1)})\|_2}{\|\mathbf{ZH}^{(2)}\mathbf{A}(\mathbf{s}_o^{(2)} - \mathbf{s}_\delta^{(2)})\|_2} \\
& \leq \frac{\|\Delta\mathbf{H}\|_F(\|\mathbf{Z}\mathbf{A}(\mathbf{s}_m^{(2)} - \mathbf{s}_{\hat{m}}^{(2)})\|_2 + \|\mathbf{Z}\mathbf{A}(\mathbf{s}_o^{(1)} - \mathbf{s}_\delta^{(1)})\|_2)}{\|\mathbf{ZH}^{(2)}\mathbf{A}(\mathbf{s}_o^{(2)} - \mathbf{s}_\delta^{(2)})\|_2}. \tag{63}
\end{aligned}$$

Since \mathbf{A} is the power constraint of generating $\mathcal{C}^{*,(2)}$, $\mathbf{A}(\mathbf{s}_o^{(2)} - \mathbf{s}_\delta^{(2)})$ can not be zero and thus the term $\|\mathbf{ZH}^{(2)}\mathbf{A}(\mathbf{s}_o^{(2)} - \mathbf{s}_\delta^{(2)})\|_2$ is non-zero. Besides, the terms ($\|\mathbf{Z}\mathbf{A}(\mathbf{s}_m^{(2)} - \mathbf{s}_{\hat{m}}^{(2)})\|_2$ and $\|\mathbf{Z}\mathbf{A}(\mathbf{s}_o^{(1)} - \mathbf{s}_\delta^{(1)})\|_2$) are generally finite. Hence, term ($\|\mathbf{Z}\mathbf{A}(\mathbf{s}_m^{(2)} - \mathbf{s}_{\hat{m}}^{(2)})\|_2 + \|\mathbf{Z}\mathbf{A}(\mathbf{s}_o^{(1)} - \mathbf{s}_\delta^{(1)})\|_2$)/ $\|\mathbf{ZH}^{(2)}\mathbf{A}(\mathbf{s}_o^{(2)} - \mathbf{s}_\delta^{(2)})\|_2$ is finite.

REFERENCES

- [1] Q. Qi, X. Chen, C. Zhong, and Z. Zhang, "Integrated sensing, computation and communication in b5g cellular internet of things," *IEEE Transactions on Wireless Communications*, vol. 20, no. 1, pp. 332–344, 2020.
- [2] C. De Lima, D. Belot, R. Berkvens, A. Bourdoux, D. Dardari, M. Guillaud, M. Isomursu, E.-S. Lohan, Y. Miao, A. N. Barreto *et al.*, "Convergent communication, sensing and localization in 6g systems: An overview of technologies, opportunities and challenges," *IEEE Access*, 2021.
- [3] T. S. Rappaport, S. Sun, R. Mayzus, H. Zhao, Y. Azar, K. Wang, G. N. Wong, J. K. Schulz, M. Samimi, and F. Gutierrez, "Millimeter wave mobile communications for 5g cellular: It will work!" *IEEE Access*, vol. 1, pp. 335–349, 2013.
- [4] H. Song and T. Nagatsuma, "Present and future of terahertz communications," *IEEE Transactions on Terahertz Science and Technology*, vol. 1, no. 1, pp. 256–263, 2011.
- [5] M. Mezzavilla, M. Zhang, M. Polese, R. Ford, S. Dutta, S. Rangan, and M. Zorzi, "End-to-end simulation of 5g mmwave networks," *IEEE Communications Surveys Tutorials*, vol. 20, no. 3, pp. 2237–2263, 2018.

- [6] X. Ge, R. Zi, X. Xiong, Q. Li, and L. Wang, "Millimeter wave communications with oam-sm scheme for future mobile networks," *IEEE Journal on Selected Areas in Communications*, vol. 35, no. 9, pp. 2163–2177, Sep. 2017.
- [7] Y. Yan, G. Xie, M. P. J. Lavery, and H. Huang et al, "High-capacity millimetre-wave communications with orbital angular momentum multiplexing," *Nature Communications*, vol. 5, no. 4876, Mar 2014.
- [8] Y. Ren, L. Li, G. Xie, Y. Yan, Y. Cao, H. Huang, N. Ahmed, Z. Zhao, P. Liao, C. Zhang *et al.*, "Line-of-sight millimeter-wave communications using orbital angular momentum multiplexing combined with conventional spatial multiplexing," *IEEE Transactions on Wireless Communications*, vol. 16, no. 5, pp. 3151–3161, 2017.
- [9] R. M. Henderson, "Let's do the twist!: Radiators, experiments, and techniques to generate twisted waves at radio frequencies," *IEEE Microwave Magazine*, vol. 18, no. 4, pp. 88–96, 2017.
- [10] X. Hui, S. Zheng, Y. Chen, Y. Hu, X. Jin, H. Chi, and X. Zhang, "Multiplexed millimeter wave communication with dual orbital angular momentum (oam) mode antennas," *Scientific Reports*, vol. 5, no. 10148, May 2015.
- [11] Y. Yan, L. Li, Z. Zhao, G. Xie, Z. Wang, Y. Ren, N. Ahmed, S. Sajuyigbe, S. Talwar, M. Tur *et al.*, "32-gbit/s 60-ghz millimeter-wave wireless communication using orbital angular momentum and polarization multiplexing," in *2016 IEEE International Conference on Communications (ICC)*. IEEE, 2016, pp. 1–6.
- [12] H. Sasaki, D. Lee, H. Fukumoto, Y. Yagi, T. Kaho, H. Shiba, and T. Shimizu, "Experiment on over-100-gbps wireless transmission with oam-mimo multiplexing system in 28-ghz band," in *2018 IEEE Global Communications Conference (GLOBECOM)*. IEEE, 2018, pp. 1–6.
- [13] W. Zhang, S. Zheng, Y. Chen, X. Jin, H. Chi, and X. Zhang, "Orbital angular momentum-based communications with partial arc sampling receiving," *IEEE Communications Letters*, vol. 20, no. 7, pp. 1381–1384, 2016.
- [14] I. A. Hemadeh, K. Satyanarayana, M. El-Hajjar, and L. Hanzo, "Millimeter-wave communications: Physical channel models, design considerations, antenna constructions, and link-budget," *IEEE Communications Surveys Tutorials*, vol. 20, no. 2, pp. 870–913, 2018.
- [15] P. Liu, M. Di Renzo, and A. Springer, "Line-of-sight spatial modulation for indoor mmwave communication at 60 ghz," *IEEE Transactions on Wireless Communications*, vol. 15, no. 11, pp. 7373–7389, 2016.
- [16] P. Liu, J. Blumenstein, N. S. Perović, M. Di Renzo, and A. Springer, "Performance of generalized spatial modulation mimo over measured 60ghz indoor channels," *IEEE Transactions on Communications*, vol. 66, no. 1, pp. 133–148, 2018.
- [17] X. Gao, L. Dai, S. Han, C. I, and R. W. Heath, "Energy-efficient hybrid analog and digital precoding for mmwave mimo systems with large antenna arrays," *IEEE Journal on Selected Areas in Communications*, vol. 34, no. 4, pp. 998–1009, 2016.
- [18] X. Gao, L. Dai, S. Han, C. I, and X. Wang, "Reliable beamspace channel estimation for millimeter-wave massive mimo systems with lens antenna array," *IEEE Transactions on Wireless Communications*, vol. 16, no. 9, pp. 6010–6021, 2017.
- [19] S. A. Busari, K. M. S. Huq, S. Mumtaz, L. Dai, and J. Rodriguez, "Millimeter-wave massive mimo communication for future wireless systems: A survey," *IEEE Communications Surveys Tutorials*, vol. 20, no. 2, pp. 836–869, 2018.
- [20] M. Kokshoorn, H. Chen, Y. Li, and B. Vucetic, "Beam-on-graph: Simultaneous channel estimation for mmwave mimo systems with multiple users," *IEEE Transactions on Communications*, vol. 66, no. 7, pp. 2931–2946, 2018.
- [21] B. Liu, C. Gong, J. Cheng, and Z. Xu, "Power allocation over broad spectra optical wireless scattering communication based on link gain correlation," *IEEE Transactions on Communications*, vol. 67, no. 10, pp. 6980–6993, 2019.
- [22] B. Liu, C. Gong, and Z. Xu, "Correlation analysis and link gain prediction for optical wireless scattering communication over broad spectra," *IEEE Transactions on Wireless Communications*, vol. 19, no. 2, pp. 1386–1396, 2020.
- [23] B. Liu, C. Gong, J. Cheng, and Z. Xu, "Correlation-based lti channel estimation for multi-wavelength optical scattering nlos communication," *IEEE Transactions on Communications*, vol. 68, no. 3, pp. 1648–1661, 2020.
- [24] T. Xiao, C. Gong, Q. Gao, and Z. Xu, "Channel characterization for multi-color vlc for feedback and beamforming design," in *2018 IEEE International Conference on Communications Workshops (ICC Workshops)*, 2018, pp. 1–6.

- [25] C.-X. Wang, J. Bian, J. Sun, W. Zhang, and M. Zhang, "A survey of 5g channel measurements and models," *IEEE Communications Surveys & Tutorials*, vol. 20, no. 4, pp. 3142–3168, 2018.
- [26] A. Maltsev, R. Maslennikov, A. Sevastyanov, A. Khoryaev, and A. Lomayev, "Experimental investigations of 60 ghz wlan systems in office environment," *IEEE Journal on Selected Areas in Communications*, vol. 27, no. 8, pp. 1488–1499, 2009.
- [27] A. Maltsev, R. Maslennikov, A. Sevastyanov, A. Lomayev, and A. Khoryaev, "Statistical channel model for 60 ghz wlan systems in conference room environment," in *Proceedings of the Fourth European Conference on Antennas and Propagation*. IEEE, 2010, pp. 1–5.
- [28] R. Chen, W.-X. Long, X. Wang, and L. Jiandong, "Multi-mode oam radio waves: Generation, angle of arrival estimation and reception with ucas," *IEEE Transactions on Wireless Communications*, vol. 19, no. 10, pp. 6932–6947, 2020.
- [29] R. Chen, H. Xu, M. Moretti, and J. Li, "Beam steering for the misalignment in uca-based oam communication systems," *IEEE Wireless Communications Letters*, vol. 7, no. 4, pp. 582–585, 2018.
- [30] G. Zheng, C. Gong, and Z. Xu, "Constrained partial group decoding with max–min fairness for multi-color multi-user visible light communication," *IEEE Transactions on Communications*, vol. 67, no. 12, pp. 8573–8584, Dec 2019.
- [31] C. Gong, Z. Xu, and J. Zhu, "Parallel channel over wide spectrum: Modeling-, mining-, and matching-based transmission optimization," *IEEE Transactions on Wireless Communications*, vol. 17, no. 5, pp. 3373–3385, May 2018.
- [32] S. Zheng, X. Hui, X. Jin, H. Chi, and X. Zhang, "Transmission characteristics of a twisted radio wave based on circular traveling-wave antenna," *IEEE Transactions on Antennas and Propagation*, vol. 63, no. 4, pp. 1530–1536, April 2015.
- [33] W. Zhang, S. Zheng, X. Hui, R. Dong, X. Jin, H. Chi, and X. Zhang, "Mode division multiplexing communication using microwave orbital angular momentum: An experimental study," *IEEE Transactions on Wireless Communications*, vol. 16, no. 2, pp. 1308–1318, 2017.
- [34] E. Basar, "Orbital angular momentum with index modulation," *IEEE Transactions on Wireless Communications*, vol. 17, no. 3, pp. 2029–2037, 2018.
- [35] C. Cai, Y. Zhao, J. Zhang, L. Wang, and J. Wang, "Experimental demonstration of an underwater wireless optical link employing orbital angular momentum (oam) modes with fast auto-alignment system," in *2019 Optical Fiber Communications Conference and Exhibition (OFC)*. IEEE, 2019, pp. 1–3.
- [36] F. Liu, M. Chen, W. Jiang, X. Jin, and Z. Xu, "Effective auto-alignment and tracking of transceivers for visible-light communication in data centres," in *Broadband Access Communication Technologies XIII*, vol. 10945. International Society for Optics and Photonics, 2019, p. 109450N.
- [37] J. Xu, "Generation of laguerre–gaussian modes by aperture or array sources," *IEEE Transactions on Antennas and Propagation*, vol. 67, no. 1, pp. 415–429, 2019.
- [38] L. Allen, M. W. Beijersbergen, R. J. C. Spreeuw, and J. P. Woerdman, "Orbital angular momentum of light and transformation of laguerre gaussian laser modes," *Physical Review A*, vol. 45, no. 11, pp. 8185–8189, Jun 1992.
- [39] M. Oldoni, F. Spinello, E. Mari, G. Parisi, C. G. Someda, F. Tamburini, F. Romanato, R. A. Ravanelli, P. Coassini, and B. Thidé, "Space-division demultiplexing in orbital-angular-momentum-based mimo radio systems," *IEEE Transactions on Antennas and Propagation*, vol. 63, no. 10, pp. 4582–4587, 2015.
- [40] H. Friis, "A note on a simple transmission formula," *Proc. IRE*, vol. 34, no. 5, pp. 254–256, May 1946.
- [41] Q. Gao, R. Wang, Z. Xu, and Y. Hua, "Dc-informative joint color-frequency modulation for visible light communications," *Journal of Lightwave Technology*, vol. 33, no. 11, pp. 2181–2188, June 2015.
- [42] Q. Gao, S. Hu, C. Gong, and Z. Xu, "Modulation designs for visible light communications with signal-dependent noise," *Journal of Lightwave Technology*, vol. 34, no. 23, pp. 5516–5525, 2016.
- [43] M. Boko and R. Dinis, "Designing good multi-dimensional constellations," *IEEE Wireless Communications Letters*, vol. 1, no. 3, pp. 221–224, 2012.